Possible climatic implications of high altitude emissions of black carbon

Gaurav Govardhan[1], Sreedharan Krishnakumari Satheesh[1,2], Ravi Nanjundiah[1,2], Krishnaswamy
Krishna Moorthy[1], and Surendran Suresh Babu[3]

[1]Center for Atmospheric and Oceanic Sciences, Indian Institute of Science, Bengaluru, India
[2]Divecha Center for Climate Change, Indian Institute of Science, Bengaluru, India
[3]Space Physics Laboratory, Vikram Sarabhai Space Centre, Thiruvananthapuram, India

Correspondence to: Gaurav Govardhan (govardhan.gaurav@gmail.com)

Abstract. On account of its strong absorption of solar and terrestrial radiations, Black Carbon (BC) aerosol is known to impact large scale systems such as the Asian monsoon, Himalayan glaciers etc., besides affecting the thermal structure of lower atmosphere. While most studies focus on the near-surface abundance and impacts of BC, our study, using online regional chemistry transport model (WRF-Chem) simulations, examines the implications of sharp and confined layers of high BC
5 concentration (called 'elevated BC layers') at altitudes of about 4.5 km and 8 km over the Indian region, as revealed in the recent in-situ measurements using high-altitude balloons. Our study demonstrates, that emissions from high-flying aircrafts are the most likely cause of these elevated BC layers. Furthermore, we show that such aircraft-emitted BC can get transported to even upper tropospheric/ lower stratospheric heights (∼17 km) aided by the strong monsoonal convection occurring over the region, which are known to overshoot the tropical tropopause leading to injection of tropospheric air mass (along with
10 its constituent aerosols) into the stratosphere. We show observational evidence for such an intrusion of tropospheric BC into the stratosphere over Indian region, using extinction coefficient and particle depolarization ratio data from CALIOP LIDAR on-board the CALIPSO satellite. We hypothesise that such intrusions of BC to lower stratosphere and its consequent longer residence time in the stratosphere would have significant implications for stratospheric ozone, considering the already reported ozone depleting potential of BC.

15 ## 1 Introduction

The important role played by atmospheric aerosol particles in global and regional climate forcing is getting increasingly accepted. The global mean net radiative forcing (including the rapid adjustments) by aerosol is estimated to be -0.9 [-1.9 to -0.1] W m^{-2} (Boucher et al., 2013), after accounting for the negative forcing by most of the aerosol species (sulphate, nitrate, sea-salts etc.) and the strong positive forcing by Black Carbon (BC), which absorbs solar radiation over a wide spectral band,
20 and to a lesser extent by dust and organics. BC, a fine particulate, is formed as a result of incomplete combustion of fossil fuels, biofuels and biomass (Kuhlbusch et al., 1996; Ramanathan and Carmichael, 2008; Bond et al., 2013). Being a strong absorber of solar and terrestrial radiation, BC heats up the atmosphere (Petzold and Schönlinner, 2004; Ramanathan et al., 2007). The global mean radiative forcing by BC is estimated as +0.4 (+0.05 to +0.8) W m^{-2}, which is around $(1/4)^{th}$ of the global mean

CO_2 radiative forcing (Boucher et al., 2013). Several earlier studies have shown that such an atmospheric heating by a layer of aerosol with high BC abundance, is capable of perturbing large scale atmospheric phenomenon such as the Asian monsoon system and can also affect the hydrological cycle (Chakraborty et al., 2004; Ramanathan et al., 2005; Lau et al., 2006). Also, on account of its absorbing nature, BC, if deposited on snow, would exert 'snow-albedo forcing' resulting from the darkening

5   of snow and could accelerate the melting of glaciers (Lau et al., 2010; Qian et al., 2011; Yasunari et al., 2010; Nair et al., 2013; Gautam et al., 2013). Furthermore, when BC particles are located above highly reflecting surfaces (such as snow/clouds), their absorption efficiency gets amplified (Haywood and Shine, 1995; Satheesh and Moorthy, 2005; Chand et al., 2009; Nair et al., 2013). This heating can give rise to local elevated dry convection, which can further lift the BC particles to higher levels of the atmosphere (de Laat et al., 2012). The atmospheric heating by BC would be more severe at higher altitudes due to reduced air

10   density at these altitudes, and this could amplify the heating effect. The high-altitude heating due to BC can also lead to reduced cloud cover at these elevated altitudes (Ackerman et al., 2000). Additionally, the atmospheric heating at higher altitude can give rise to local stable scenario below, which can affect convection and consequently impact precipitation. The aforementioned effects highlight the significance of knowing the vertical distribution of BC especially over regions of strong convection (such as the Indian subcontinent especially during the pre-monsoon and the monsoon months). With this backdrop, a few studies

15   have examined the vertical distribution of aerosols (extinction coefficient values and/or BC mass concentration values) over the Indian region using multiple observational platforms such as a ground based LIDAR (Satheesh et al., 2006), airborne and space based LIDAR (Satheesh et al., 2008; Prijith et al., 2016), instrumented aircrafts (Moorthy et al., 2004; Babu et al., 2008, 2010; Nair et al., 2016), tethered and high-altitude balloons (Babu et al., 2011). Carrying out such observations for the first time over India, Moorthy et al. (2004) have noticed an exponential decrease of BC concentration within the boundary

20   layer and a steady value above it, over an urban station (Hyderabad) in south-central India during the month of February, 2004. Examining the vertical profile of aerosols over Bangalore (an urban station in southern part of India) using a ground based micro pulse LIDAR, Satheesh et al. (2006) have reported morning-time (night-time) vertical lifting (confinement) of aerosols during summer days. Carrying out airborne measurements of BC and absorption coefficient over several stations across India, Babu et al. (2008, 2010); Nair et al. (2016) have reported a near-steady vertical distribution up to an altitude of

25   3 km above ground, with isolated peaks of higher BC concentration/ absorption coefficient during pre-monsoon period, above most of the landmass. Synthesizing multi-platform measurements Satheesh et al. (2008) have revealed the existence of elevated aerosol layers in the middle troposphere. They have shown that these elevated aerosol layers caused atmospheric heating, which exhibited a meridional gradient that varied in vertical extent and amplitude from the northern Indian Ocean to Central India, during the pre-monsoon season. Using hydrogen inflated zero pressure balloon measurements for the first time in India,

30   Babu et al. (2011) have revealed strikingly sharp and confined layers of BC at altitude of 4.5 km and 8 km over Hyderabad during the pre-monsoon season of 2010. They also have reported a large decrease in the environmental lapse rate associated with these peaks, using concurrent measurements aboard the same balloon. Analysing multi-year satellite (CALIPSO) data, Prijith et al. (2016), not only confirmed the existence of high altitude aerosol layers and their meridional gradient in the vertical extent during pre-monsoon periods over Indian region, but also have shown that mineral dust aerosol forms the dominant

35   component of this layer. Kompalli et al. (2016) have reported spring-time enhancement in columnar Aerosol Optical Depth

(AOD) and BC over Hanle – a western trans-Himalayan high-altitude observational location (4.5 km amsl). They attributed this enhancement to summer-time lifting of aerosols over the region west to south-west of Hanle and subsequent long-range transport. All the above studies clearly bring out the existence of high altitude aerosol layers (with significant amount of BC) over the south Asian region during the pre-monsoon periods. Such strong absorbing aerosol layers can perturb the south Asian

5   regional monsoonal system and can also affect the glacial coverage of the south Asian region. Thus, it becomes imperative to understand the dynamics of this regional high altitude aerosol layers and investigate the exact causes behind their occurrence.

In this study, we revisit the three high-altitude balloon measurements of BC made during the years 2010, and 2011, (in different seasons) over Hyderabad (the only location in India from where such balloon ascents could be made) and investigate the potential causes behind the existence of such confined BC layers, using a regional chemistry transport model. The balloon

10 experiments and profiles are described in section 2, the model and simulation details are described section 3 and in section 4, we discuss the results. The possible climatic implications of such high-altitude BC layers are discussed in section 5. The conclusions are presented in section 6.

2   High altitude measurements of BC

The vertical profiles of BC used in this study have been obtained using an Aethalometer (Model AE-42, of Magee Scientific,

15 USA), aboard high-altitude zero pressure balloons, launched from the National Balloon Facility at Hyderabad, (17.48^{0}N, 78.47^{0}E, 557 m amsl), during three ascents made on 17 March 2010, 08 January 2011 and 25 April 2011. The first and third flights corresponded to pre-monsoon conditions, while the second flight occurred in winter. The details of experimental set-up, calibration, data collection and analysis are available in Babu et al. (2011) and as such, only a brief account is given here. The 109755 m^3 zero-pressure balloon was made of 25 mm thick, linear low density polyethylene film, and was capable of carrying

20 ∼350 kg of payload up to a ceiling altitude of ∼35 km. Besides the aethalometer, each ascent also carried other payloads such as GPS receiver, meteorological sensors for temperature and RH, telemetry and telecommand systems. The aethalometer had been configured for volumetric flow with an external pump, providing a flow rate of 14 liters per minute (LPM) at ground, and operated at a time base of 5 s. The entire payload was tested using a thermo-vacuum facility to ensure consistent operations up to ∼9 km altitude (250 hPa pressure level and ∼ -40^{0}C). Beyond this altitude, as the ambient pressure drops too low to provide

25 sufficient flow to the aethalometer, the telecommand system was used to switch off the instrument for the higher altitudes, and switch it on again at this altitude during the descent phase. A gondola, carrying the payloads, had been attached to the balloon using a parachute, which was deployed in the descent phase and enabled safe recovery of the payloads for reuse. Ballast cans attached to the gondola ensured a slow and steady ascent of ∼2.6 m s^{-1}, while the descent speed was controlled by the parachute, as the ballast cans were detached after the balloon rose to the free tropospheric altitude. The scientific data

30 along with the housekeeping data were collected during the ascent and descent phases and were continuously telemetered to the ground, besides storing on-board. The total flight duration was about 3 to 4 hours and the spatial ground spread of the flight path has been within 50 km radius of the launch site. The data have been analysed (following details in Babu et al. (2011)) and the profiles obtained were smoothed using a running mean filter. The same protocols have been followed for all

the flights. The vertical profiles of BC, derived from these flights are shown in fig.1, in which each profile is the average of the ascent and descent profiles for that flight. All the profiles revealed sharp and confined peaks in BC concentration in the free troposphere above a near-steady mass concentration within the planetary boundary layer ($\sim$ 2 km for pre-monsoon and $\sim$ 1km for winter). These peaks are identified on the respective profiles in fig.1. It is also seen very clearly that the sharp and most

5 prominent peak occurred at between 4 and 5 km in the first and last profiles (fig.1a and fig.1c); which incidentally correspond to the pre-monsoon flights, while it occurred at a slightly lower altitude (between 2 to 3 km) in the winter profile. The highest altitude layer seen in the profiles were in the vicinity of 7-9 km, though the amplitudes of these are much smaller than that of the layer seen at around 4.5 km. With the help of temperature data from the collocated meteorological payloads, we evaluated the environmental lapse rate profile for each of these profiles and the mean profile for each flight is shown in fig.2, following

10 the same order as in fig.1. It is clearly seen that in the vicinity of the prominent BC peaks (P1 to P5 in fig.1a-c) there is a large reduction in the environmental lapse rate (sometimes reaching close to zero) e.g. at 4.5 km during March 2010 (fig.2a), around 2-3 km and 7 km during January 2011 (fig.2b); and around 4-5 km and 6-7 km during April 2011 (fig.2c). The lapse rate profile during April 2011 (fig.2c) shows multiple spikes possibly due to higher number of peaks in the corresponding BC profile (fig.1c), (Since the raw temperature data is very noisy, we have smoothened the data using two points fixed and

15 two points moving average filter). Such reductions in temperature lapse rate would affect the local stability scenario. While the occurrence of high BC below 3 km can be explained by the boundary layer dynamics, high BC values at higher levels especially at 7 to 9 km, remained a mystery. Babu et al. (2011) hypothesized that the occurrence of such BC peaks at high altitudes could be associated with the local sources of BC at those altitudes, as 4-5 km and 8-9 km are the preferred corridors for aircrafts flying over Hyderabad. With a motivation to test this hypothesis and also to estimate the climate implication of such BC layers, we in

20 this study, investigate the causes for the occurrence of such sharp and confined BC peaks at higher altitudes, using a regional online chemistry transport model. Crucial findings from this study are reported and possible ramifications are discussed.

3   Model and simulation details

The WRF-Chem model used in this study employed horizontal grid spacing of 2 km with 70 vertical levels and 100 m vertical resolution around the layers 4-6 km, 8-9 km and 10-11 km. Such a high vertical resolution was chosen to resolve the BC peaks, if simulated by the model, accurately. The model domain (75.5^0E- 80.5^0E, 14.5^0N- 20.5^0N) centers at Hyderabad and spans

25 around 330 km in each direction (See fig.3 for details.). The simulations were started 16 days prior to the balloon flight days (flight day 1: 17 March, 2010, flight 2 : 8 January 2011 and flight day 3: 25 April 2011) and were run till the end of the flight day. In these simulations, the convective processes were not parameterized due to the fine grid spacing; cloud microphysical processes were parameterized using the Thompson scheme (Thompson et al., 2004), boundary layer processes were param-

30 eterized using the YSU scheme (Hong et al., 2006; Hong, 2010), and the surface processes were modeled using RUC-LSM scheme (Smirnova et al., 1997, 2000). The short-wave radiation processes were parameterized using Dudhia scheme (Dudhia, 1989) while the long-wave processes were parameterized using RRTM (Mlawer et al., 1997). Gas-phase chemistry in these simulations was handled by MOZART mechanisms (Emmons et al., 2010), while the aerosol-phase chemistry was parameter-

ized using GOCART bulk aerosol scheme (Chin et al., 2002) with Fast-J scheme for photolysis (Wild et al., 2000).

The model takes into account the following aerosols species: BC1 (Hydrophobic), BC2 (Hydrophilic), OC1 (Hydrophobic), OC2 (Hydrophilic), Dust (5 bins: effective diameters from 0.5 to 8 μm), Sea-salts (4 bins: effective diameters from 0.1 to 7.5 μm) and sulphate. The model simulates aerosol transport processes like emissions, advection, diffusion and deposition

5 (dry and wet). The aerosol direct effects are modeled by coupling the aerosol scheme with the radiation scheme. The NCEP FNL (Final) Operational Global Analysis data, (interpolated to model resolution) has been used for setting up the initial and boundary conditions (updated every 6 h) for meteorological variables in the model, while the global chemistry transport model MOZART-4 (Emmons et al., 2010) has been used for creation of initial and boundary conditions for chemistry variables. The near-surface emissions of gas-phase as well as aerosol-phase species are formulated using the standard emission pre-processor

10 software PREP-CHEM-SRC (version 1) (Freitas et al., 2011). The RETRO database (Schultz et al., 2007) is used for various greenhouse and precursor gases, EDGAR (Olivier et al., 1996) for emissions of CO, NO, NH_3 and VOCs and the GOCART (Chin et al., 2002) database is used for the emissions OC, BC and SO_2 over the region. The necessary modifications in BC emissions from GOCART database over this region (Govardhan et al., 2016) have been incorporated. We conducted two sets of simulations for each of the events. The first set included only surface emissions (NoACEM/Ctrl (Control) run) and the second

15 set included surface and elevated emissions (ACEM, details of elevated emissions are discussed in section 4.3)

4   Results and Discussions

4.1   Meteorological evaluation of the model

Meteorological processes like advection, diffusion, deposition etc. play a significant role in controlling the concentration of pollutants near the surface and their vertical distribution in the troposphere (Govardhan et al., 2015). Hence, before inspecting

20 the model simulated vertical profile of BC, we first examine the performance of the model in simulating meteorology over the region of interest. We show such comparisons for March 2010 NoACEM simulations as a representative one. The model simulated meteorological parameters are averaged over the balloon flight region and then compared with the corresponding observations from the balloon flight. The three-point running mean smoothing is used to smoothen observational and simulated vertical profiles. Firstly, we have compared the model simulated vertical profile of horizontal wind speed (Blue line, fig.4 a)

25 and direction (Blue line, fig. 4b) with the corresponding observations (Red line, fig.4a and Red line, fig.4b) available from the balloon flight measurements (deduced from the GPS data on board the balloon). The figures depict relatively weak (less than 10 m s^{-1}) low-level northerly-northeasterly winds upto around 5 km. Beyond this altitude, the winds change direction gradually and become westerlies above 8 km. The wind speeds also increase drastically beyond 8 km and reach a value of 20-25 m s^{-1} at a height of 9 km and beyond. While the model simulated vertical variation of wind speed (Blue line, fig.4a) and direction (Blue

30 line, fig.4b) agree broadly with the measurements, they differ in details and magnitudes. In model simulations, the change in wind direction starts occurring at an altitude $\sim$ 1 km lower than in observations. The large increase in wind speed beyond 8 km altitude is satisfactorily captured by the model. Thus, with some disagreements in the actual magnitudes, the model captures broad features of horizontal advection strength (wind speed) and nature (wind direction) over the balloon flight domain vis-

a-vis the measurements. We next examine the model simulations of vertical stability over the flight domain by comparing the model-simulated vertical profiles of potential temperature (θ) with the corresponding profiles from the balloon data. The observed profile (Red line, fig.4c) shows a stable layer (θ increases with height) up to 1st 2 km of the lower troposphere. Above this layer, there occurs a thick, well-mixed layer upto a height of 4 km, in which θ remains almost height-invariant. Above this

5   height, the atmosphere remains largely stable with increase in θ with height. The modeled altitude variation of θ (Blue line, fig.4c) in general, matches with the measurements, barring a few discrepancies such as the extent of stable and well mixed layer in the lower atmosphere, magnitude of θ in the vicinity of the primary BC maxima in observations (around 4-4.5 km, fig.1a) etc.. The model captures the stable layer lying up to around 1.5 km, similar to that seen in observations (up to 2 km, red line, fig.4c). A convectively unstable, well-mixed layer (θ constant) extending upto a height of 3.5 km, occurs above this layer,

10   akin to observations (up to 4 km, red line, fig.4c), with an underestimation in θ values. Beyond this height, model also does not show any sign of instability, while θ increases with height, in agreement with the observations, yet with differences in the magnitudes. Thus, the model simulated vertical profile of θ also appears to be broadly comparable to the observed profile, with some differences. Examining the vertical thermal structure, we have also compared the model simulations of vertical profile of temperature with the corresponding measurements from the flight. While showing in general reduction in temperature with

15   height similar to the observations (Red line, fig.4d), the model (Blue line, fig.4d) shows discrepancies in actual magnitudes vis-a-vis the observations, as in case of the other meteorological variables. Possibly, owing to the existence of the primary BC peak between 4 to 5 km, the observations (Red line, fig.4d) depict a near-steady temperature within the particular altitude layer. The model (Blue line, fig.4d) on the other hand, fails to capture this feature. Thus, along with some differences in the details, the model simulations capture some of the large-scale features of the meteorology over the balloon flight region vis-a-vis the

20   observations.

4.2   Simulated vertical profile of BC

With the above broad agreements in the meteorological fields, we proceeded to examine and evaluate the model simulated vertical profile of BC over the balloon flight domain (fig.5a). For 17th March 2010, the model simulations, though successfully capture the nature of the altitude distribution of BC, there are considerable differences in the finer details, vis-a-vis the obser-

25   vations (fig.1a). The magnitudes of the simulated BC significantly match the observations only over the lower most altitudes i.e. below 3.5 km. Above that altitude, the 2 profiles completely differ from each other; while the observations (fig.1a) show an increase in BC followed by a sharp peak at 4.5 km (BC > 12 μg m^{-3}), the model (fig.5a) displays a rapid decrease in BC concentration with altitude, without even a sign of the 'elevated' (high altitude) layers of high BC concentration seen in the measurements. Thus, though the model satisfactorily simulates the meteorology over the flight domain, it does not simulate

30   the observed vertical profile of BC beyond 4 km altitude. The results for the other two flights are shown in fig.5b and fig.5c. During January 2011, the model simulations (fig.5b) show rapid reduction in BC beyond 1 km. There is no sign of sharp and confined peaks beyond this height unlike the corresponding observations (fig.1b). During April 2011, the model simulations (fig.5c) show sharp reduction in BC in first 1 km. Beyond this height, the BC concentration remains relatively steady with height upto 3 km, above which a small peak is indicated between 3-4 km followed by a flat steady BC profile with very low

values above that height. Thus, even during April 2011, though the model satisfactorily captures the BC variations upto 3-4 km, it fails to do so at higher altitudes. Thus, none of the model simulations capture the sharp-confined BC peaks (or the elevated BC layers) occurring at higher altitudes. This strongly suggests that the meteorological factors alone cannot be responsible for the existence of the elevated BC layers. To throw more light on this, we considered other hypothesis.

5   The meteorology (observed as well as simulated) being benign for all the cases, and possibility of any long-range transport of BC from other location being an unlikely cause for such high concentrations, one has to look for local injection of BC aerosols at mid and upper troposphere because, surface based emissions would not lead to elevated BC layers at altitudes of 4-5 km or 7-9 km. In this context, emissions from commercial air traffic (that overfly Hyderabad, as well land and take off from there) assume significance. In their first reporting of the elevated layers, Babu et al. (2011) have hypothesized the role of

10   such emissions, where they have obtained an approximate estimate of air traffic over the study location; about 200 aircrafts that overfly Hyderabad in the corridor 8-10 km and another 250 to 300 km that use the corridor 4 to 5 km, in the course of landing and taking off from the airport. We next evaluate elevated emissions due to aircrafts as a likely candidate for these high concentrations.

4.3   Prescription of aircraft BC emissions

15   For this, we prescribed aircraft BC emissions from the MACCity global anthropogenic emissions inventory (Lamarque et al., 2010) in the WRF-Chem simulations. The inventory provides aircraft BC emissions at $0.5^0 \times 0.5^0$ grids and 23 vertical levels from 0.305 km to 13.725 km, with a vertical resolution of 610 m. The basic information this inventory considers are: global aircraft movements, performance characteristics of the different aircraft types, the actual paths of aircrafts during their journey and the emission factor for BC per kg of aviation fuel burnt. This global inventory for aircraft BC emissions inherently have

20   several uncertainties, especially over a region like India mainly due to uncertainties associated with a) amount of total aircraft fuel used across the country by domestic and international fleets; b) quality of aircraft fuel; c) age of aircrafts and hence the degradation in performance; d) exact number of civil aircrafts flying over the region e) unaccounted military aircrafts and f) exact routes followed by the aircrafts over this region. Additionally, a major source of uncertainty in the estimates of BC emission from aircrafts arises due to the uncertainties in the estimations of emission factor for BC 'EI(BC)' for the

25   particular aircraft fuel being used. EI(BC) is the amount of BC emitted (in g) per kg of aircraft fuel burnt and it depends on engine type, load conditions, engine conditions etc.. The measurement of EI(BC) by several studies (Herndon et al., 2008; Onasch et al., 2009; Timko et al., 2010) indicate that EI(BC) spans around four orders of magnitude. Stettler et al. (2013) discuss and quantify the underestimation of EI(BC) observed in currently available aircraft BC emissions inventories. In a previous study (Stettler et al., 2011) have stated: "The First-Order Approximation (FOA3) - currently the standard approach

30   used to estimate particulate matter emissions from aircraft - is compared to measurements and it is shown that there are discrepancies greater than an order of magnitude for 40% of cases for both organic carbon and black carbon emissions indices". Thus, considering such underestimations of EI(BC) in the current emissions inventory, we modified the emissions and forced our model with such emissions at 23 levels with appropriate mapping to model levels.

4.4 Simulated vertical profile of BC with aircraft BC emissions

We examine the outcome of prescription of BC emissions from aircrafts on the modeled vertical profile of BC in fig.6, averaged over a region 8 km^2, in the vicinity of the balloon flight location, for the 3 balloon flight days. It is quite interesting to note that, upon the prescription of BC emissions from aircrafts, the model simulations (ACEM- simulations with the prescription

5 of AirCraft EMissions) show sharp layers in the vertical profiles akin to the observed BC profiles (fig.1.), which are not simulated otherwise (NoACEM/Ctrl (control) run- simulations without the prescription of AirCraft EMissions). Though the actual altitudes and the magnitude of the BC layers differ in comparison with the observations, the nature of the layers (sharp and confined) looks very similar to those seen in the measurements. The two peaks in BC profile during March, the lower and the upper level BC peaks during January and the clustered BC peaks during April are well simulated by the model only

10 after the prescription of BC emissions from aircrafts. Thus, even for the model with realistic meteorology, the high altitude BC peaks/ layers are captured only when the high altitude sources of BC are prescribed. This clearly highlights the role played by aircraft emissions of BC in creation of the high altitude BC peaks, which remained as a hypothesis earlier. Additionally, as a consequence of such high altitude BC emissions , the modelled vertical profile of temperature lapse rate over the balloon flight region shows a reduction in the magnitude in ACEM case as compared to the NoACEM case, indicating the warming due to BC

15 (fig.7a). The corresponding differences in the temperature lapse rate (d(dT/dz)= (dT/dz)$_{ACEM}$ - (dT/dz)$_{NoACEM}$) appear to be higher especially at higher altitudes of 4 km and beyond 7km (fig.7b). Such a reduction in the magnitude of the temperature lapse rate values, results in a better match between model simulations and the corresponding observations of temperature lapse rate especially at higher altitudes (from 6 to 8 km and from 9 to 9.5 km)(fig.7a). Additionally, we carried out one more model simulation, in which we prescribed the emissions of BC from biomass burning activities using FINN-version 1.5 inventory

20 (Wiedinmyer et al., 2011) biomass burning data. This Fire INventory from NCAR (FINN) provides high resolution, global emission estimates from such open burning activities. The temporal resolution of the inventory is 1 day, while the spatial resolution is 1 km^2. In our simulations, we allowed such emissions from biomass burning to lift vertically following the online plume-rise module (Freitas, 2007). However, the model could not simulate the observed sharp and confined BC peaks (figure not shown), if we switch off the prescription of BC emissions from aircrafts. This clearly shows the important role of aircraft

25 BC emissions in causing high altitude BC peaks.

4.5 Sensitivity of the vertical profile of BC to the surface level emissions

To test the robustness of the simulated high altitude BC peaks, we have also examined the impact of near-surface emissions of BC on the elevated layers. For this, we have done a similar simulation with aircraft BC emissions, in which we have turned-off the near-surface fossil fuel emissions of BC over the model domain. We have then examined the effect of this on the simulated

30 vertical profile of BC in fig.8. It can be clearly seen from this figure that the vertical profiles simulated by the 2 runs (SE- the run with prescribed near-surface anthropogenic emissions of BC and N-SE – the run with near-surface anthropogenic BC emissions turned off) differ only in the lower altitude region, upto a height about 4 km (probably the altitude up to which BC could be lofted by the convection). Beyond 4 km, the profiles are identical, implying that the elevated BC layers are insensitive to surface

BC emissions. Thus, our model simulations indicate that, the high altitude peaks in BC are not a result of convective-lifting of near-surface BC, but they are indeed caused due to the BC emissions (injection of BC) at higher altitudes by the aircrafts.

4.6 Atmospheric heating rate due to the observed and modelled BC vertical profile

Being a strong absorber of radiation over a wide spectral band, elevated BC layers absorb incoming solar, which would then heat-up the atmosphere locally and can alter the vertical stability. In this section, we compute the atmospheric heating caused by the observed and modelled BC vertical profiles. The methodology that we follow to compute the atmospheric heating rates due to BC is similar to that followed by Babu et al. (2002) and Babu et al. (2011).

4.6.1 Atmospheric heating rates due to observed BC

The atmospheric heating rates due to the observed vertical profiles of BC are computed using a Discrete Ordinate Radiative Transfer Model (Santa Barbara DISORT Atmospheric Radiative Transfer - SBDART (Ricchiazzi et al., 1998)). SBDART solves radiative transfer equations considering a plane-parallel atmosphere. Aerosol are included in SBDART by specifying total aerosol optical depth, single scattering albedo (SSA) and the Legendre moments of the scattering phase function for the assumed aerosol mixture; at every vertical layer. The required layer-wise total AODs were computed using vertical profile total extinction coefficient from CALIOP (Cloud Aerosol Lidar with Orthogonal Polarization) LIDAR on-board the CALISPO (Cloud Aerosol Lidar Pathfinder Satellite Observation) satellite. The level 2 extinction coefficient data from CALIPSO was cloud-screened using the standard, recommended cloud-screening algorithm (https://www-calipso.larc.nasa.gov/resources/calipso_users_guide/tools/index.php) which makes us of the flags like AVD (Atmospheric Volume Description), CAD-Score (Cloud Aerosol Detection- Flag), extinction coefficient uncertainty and extinction coefficient quality control to separate aerosol from clouds. The final vertical profile of extinction coefficient considered was the mean all such cloud-screened vertical profiles which fall within $\pm 1.5^0$ of the balloon flight location in x-y direction and also ± 20 days of the balloon flight date. Such an averaging was done to get a mean picture of the aerosol loading over the balloon flight region. To get the required single scattering albedo we made use of the observed vertical profile of BC and the OPAC (Optical Properties of Aerosol And Clouds) model (Hess et al., 1998). OPAC provides optical properties like extinction coefficient, absorption coefficient, scattering coefficient, single scattering albedo, asymmetry parameter, phase function etc. for the prescribed mixture of aerosol species. In OPAC, we prescribed the measured vertical distribution of BC to get the corresponding absorption coefficients. These absorption coefficients along with extinction coefficients from CALIPSO were used to get SSA. Finally, in order to compute the Legendre moments of the scattering phase function, we execute OPAC with one of its preset aerosol mixture- 'urban'; as it is best-suited for our observational location . This aerosol mixture has water soluble species (28000 # cm^{-3}), insoluble species (1.5 # cm^{-3}) and soot (130000 # cm^{-3}). For the 'urban' aerosol mixture we derived the scattering phase function and computed 8 Legendre moments of the scattering phase function. Along with the aforementioned primary inputs, SBDART requires some additional inputs such as mean state of atmospheric variables viz. temperature and pressure on every vertical level; and vertical profile of specific humidity and ozone. These inputs were taken from SBDART database under 'tropical' category, which suits our observation location (Hyderabad). Additionally, spectrally varying surface albedo values for Hyderabad were taken from

MODIS surface reflectance product (MOD09CMG). This daily level 3 product provides surface reflectance for 7 bands (469 nm, 555 nm, 645 nm, 858.8 nm, 1240 nm, 1640 nm and 2130 nm) at 0.05^0 resolution. With all these inputs SBDART model was executed with 8 streams in the radiative transfer calculations with 7.5^0 resolution for solar zenith angle varying from 0 to 180. The net radiative fluxes were computed at top and bottom of every vertical layer starting from surface to 100 km. A

5   similar run of SBDART was conducted without the prescription of aerosols. Using radiative fluxes from these 2 runs, radiative forcing within each layer was estimated using

$$\Delta F = Flux_{NA} - Flux_A \qquad (1)$$

where, $Flux_{NA}$ = Radiative flux in absence of aerosols (W m^{-2})

$Flux_A$ = Radiative flux in presence of aerosols (W m^{-2})

10   The change in radiative fluxes in each layer due to aerosol is the amount of energy absorbed in the layer due to aerosols. Corresponding atmospheric heating rates were computed using Liou (2002),

$$dT/dt = (g/Cp)(\Delta F/\Delta p) \qquad (2)$$

where dT/dt is the heating rate (K s^{-1}), g is the acceleration due to gravity, Cp the specific heat capacity of air at constant pressure (Cp=1006 J kg^{-1} k^{-1}) and p is the atmospheric pressure. (Satheesh and Ramanathan, 2000). The heating rates (K

15   day^{-1}) were then averaged for 24 hours.

Following the aforementioned procedure we computed the atmospheric heating rates due to the measured BC profiles for the 3 balloon flights. The heating profiles are presented in fig.9a, fig.9b and fig.9c for the March, January and April flights respectively. The vertical extent of the profiles is limited to the availability of the extinction coefficient data from CALIPSO satellite. During March 2010 (fig.9a), the heating rates are seen to be within 0.5 to 1 (K day^{-1}) upto 2-2.5 km of the atmosphere.

20   The denser atmosphere could also be one of the factors responsible for such low values of heating rates at lower altitudes. Beyond this height, a large increase in heating rates could be seen up to $\sim$5 km. The heating rate maxima ($\sim$5 K day^{-1}) is seen to occur around the height of BC maxima (fig.1a). Such a large heating rate could cause the observed reduction in temperature lapse rate around those altitudes (fig.7a). During the winter flight (January 2011, fig.9b), the observed BC profile causes more heating near the surface than that at higher heights. The corresponding heating rates at near-surface levels are even higher than

25   that during the summer months (March 2010, fig.9a and April 2011, fig.9c). The heating rate profile during April 2011 (fig.9c) shows similar features as that of March 2010 (fig.9a). The maxima in heating rate also occurs around the elevated BC layers, with comparable magnitudes. As expected, since the observed BC profile during April 2011 (fig.1c) shows more number local peaks as compared to that during March 2010 (fig.1a), the heating rate profile during April 2011 also shows more pronounced spikes vis-a-vis March 2010. The identical nature of the heating rates profiles during March 2010 and April 2011, brings out

30   the average features of heating rate profile during summer months over the region of study. Thus, during the summer months the study region is characterized with maxima in the heating rates ($\sim$5 K day^{-1}) at around 4-5 km, while during the winter months the maxima ($\sim$1 K day^{-1}) lies near the surface.

4.6.2 Atmospheric heating rates due to modelled BC

The vertical extents of heating rate profiles from the measurements were limited due to the availability of extinction coefficient data from CALIPSO over the region of interest. Such a limitation does not exist for model data, hence we now compute the atmospheric heating rates using the model results. To compute the atmospheric heating rates using model data we follow exactly the same procedure that was used earlier. The only differences are: we now use extinction coefficient data from model simulations instead of the CALIPSO satellite and we use SSA from model simulations instead of deriving it from the observed BC. The corresponding atmospheric heating rate profiles in model simulations are shown respectively in fig.10a,b and c. The heating rates are computed for the corresponding BC profiles (ACEM) shown in fig.6a,b and c. The profiles are averaged for a region 8 km^2 and are representative of all such profiles, which show the effect of aircraft emissions. During March 2010, the model heating-rate profile (fig.6a) shows similar features vis-a-vis the corresponding observations (fig.9a). Though the actual magnitudes of heating rates are lower for the model simulated profiles, it captures the major and important features such as steady increase in heating rates from surface to 3 km and maxima in heating rates at around 3-4 km. Interestingly, a secondary peak in heating rates can be seen around 11 km. This peak corresponds to the peak in BC as seen in fig.6a. During January 2011(fig.10b), the model also shows high values of heating rates nearer to the surface similar to the observations (fig.9b). Beyond this height the heating rates reduce. A secondary peak in heating rates at around 10-12 km is seen also during January 2011, with the magnitude as high as 0.5 K day^{-1}. During April 2011, the model heating rate profile (fig.10c) shows a maximum close to the surface corresponding to the maximum in BC (fig.6c), and multiple maxima at higher heights (3km, 6km) corresponding to the presence of BC layers. The upper level maxima at around 11 km is seen to be relatively weaker during April (fig.10c) vis-a-vis March (fig.10a) and January (fig.10b) simulations. The heating rate profiles shown in fig.10a-c, are a representative of all those locations which show an existence of the aircraft emitted BC trails at higher altitudes, but are located away from the starting point of the trail (We entitle 'starting point of the trail' as that area in the aircraft emitted BC trail, where emission magnitudes are substantially higher than that over the remaining part of the trail). We term these generic heating rate profiles as 'normal profiles'. Additionally, we inspected the heating rate profiles for those locations which lie in the vicinity of the starting point of the trails. We term these heating rate profiles as 'extreme profiles'. Such 'extreme profiles' of heating rates are shown in fig.10d-f, for March 2010, January 2011 and April 2011 respectively. It can be noticed from fig.10a-f that, while the extreme profiles show similar heating rate magnitudes within lower part of the atmosphere as that of the normal profiles; they produce very high heating rates at the higher heights (10-12 km). Such heating rates even cross the near-surface maxima for the April 2011 profile (fig.10f). The rarer atmosphere could also contribute to such a high values of heating rates at those altitudes. Such large heating rate values at those heights can affect the stability of the atmosphere. The resulting vertical mixing can lift the BC particles even higher. This continuous warming-lifting cycle can result in further vertical transport of the BC particulates, which is termed as self-lifting of BC (de Laat et al., 2012). In addition to the self-lifting mechanism, the BC emitted at high altitudes can get transported vertically up in presence of strong underlying convection. In the next section, we show, with the help of model simulations, that such convective transport of the high-altitude BC could occur in tropics during periods of strong convection.

4.7 Convective lifting of BC

To examine the convective lifting of high-altitude BC, we have carried out WRF-Chem simulations with the prescription of aircraft BC emissions over Indian region for July 2010. July month was selected for this purpose, in view of the known prevalence of deep convection over Indian region, associated with the summer monsoon and the tropical tropopause layer

5   being thinnest at this time of the year (Meenu et al., 2010; Sunilkumar et al., 2013). The tropical tropopause layer is the region between the top of the major convective towers and the cold point. While forming an interface between the two dynamically different regimes, this layer acts as an entry-point to the tropical stratosphere (Fueglistaler et al., 2009). The animation (Mov.1 in supplementary material) shows height-longitude plots of maximum value of BC for a latitude belt of 2.25^0 over Hyderabad (X-axis: Longitude, Y-axis: Height (m)). The animation clearly reveals the capability of strong convections to lift BC to heights

10   beyond 14 km. On a few occasions, these layers are seen to get transported even beyond 17 km, across the tropopause. Similarly, we compute the difference in the upper tropospheric BC mass concentration values in ACEM (runs with the prescription of aircraft BC emissions) simulations vis-a-vis the NoACEM case (runs without prescription of aircraft BC emissions) (ΔBC= BC_{ACEM}-BC_{NoACEM}), averaged for the entire duration of model simulations carried out during July 2010. The maximum of such time-averaged ΔBC values across the latitude belt of 2.25^0 centered over Hyderabad, for every longitude of the model

15   domain is shown in fig.11. The time-averaged increment in UTLS (Upper Troposphere and Lower Stratosphere) BC load due to aircraft BC emissions is seen to occur over the entire longitude belt, though more pronounced over a few longitude bands (79^0E-80^0E). Higher ΔBC values extend vertically even beyond 17.6 km, highlighting the mean vertical transport of aircraft emitted BC in the UTLS region. These provide a strong evidence for the intrusion of high altitude aircraft emitted BC into the upper-tropospheric-lower-stratospheric heights over the Indian region during strong convective periods. Similar lifting of

20   pollutants due to convection to stratospheric heights has also been reported by some of the earlier studies (Andreae et al., 2001; Fromm et al., 2005; Randel et al., 2010; Vernier et al., 2011). The intrusion of such tropospheric air into the stratosphere will be favored under certain conditions like thinner tropopause layer, unstable conditions within the tropopause layer etc. Examining the long term records of tropopause characteristics over Indian region using the vertical profiles of temperature obtained from radiosonde measurements at thirty-four different India Meteorological Department (IMD) stations, for the period

25   1994–2011, Sunilkumar et al. (2013) have reported thinning of the Tropical Tropopause Layer (TTL) over the region during monsoon season occurring mainly due to strong monsoonal convection. The TTL thickness goes down to ~2.5 km during July-August, from ~3.5 km during December-January. Also, during monsoon season, the Temperature Lapse Rate (TRL) within TTL increases to ~ -6 K/km from its value of ~ -5.4 K/km during the other months. Such a rise in TLR make TTL more convectively unstable and favorable for vertical lifting of air parcels. Thus, the reduction in TTL thickness and increase in TLR

30   within TTL during monsoon season create favorable conditions for cross-tropopause transport of air and pollutants. A recent study by Das et al. (2016) reports a cross tropopause transport of air-mass over Indian region during the cyclone 'Nilam'. Such a cross-tropopause transport coupled with convective transport/self-lifting of high altitude aircraft emitted BC to higher heights, lends strong support to the stratospheric intrusion of BC particles. Once the particles enter the stratosphere, they reside

for a longer period of time due to the inherent stability of stratosphere and the absence of strong removal mechanisms. In the next section, we show observations supporting such intrusion.

4.8 Occurrence of BC at high altitudes: Observational evidence

There exist several observational reports of presence of BC at upper tropospheric and the stratospheric altitudes (Chuan and Woods,
5   1984; Okada et al., 1992; Pueschel et al., 1992; Sheridan et al., 1994; Blake and Kato, 1995; Pueschel et al., 1997; Strawa et al., 1999; Baumgardner et al., 2004; Schwarz et al., 2006; Kremser et al., 2016). One of the ways to ascertain the occurrence of such layers in the stratosphere is to examine the CALIOP LIDAR (on board CALIPSO satellite) extinction coefficient data (at 550 nm). We have examined all such vertical profiles for 3 consecutive years (from January 2010 to December 2012), over 5 specifically chosen regions ($5^0 \times 5^0$) over and around India (fig.12). Since, we want to focus on the presence of aerosols
10 at stratospheric altitudes, we have plotted the vertical profiles of extinction coefficient in the stratospheric altitudes (i.e. from altitude 20 km to $\sim$ 30km). The results are shown in fig.13.

To our surprise, we notice that the aerosol extinction coefficient values over the stratospheric altitudes are more than 0.02 km^{-1} over all these regions; occasionally values greater than 0.06 km^{-1} are also noticeable (fig.13a). The corresponding appended time-series of stratospheric (i.e. from altitude 20 km to $\sim$ 30km) Aerosol Optical Depth over the regional boxes under
15 consideration from 2010 to 2012 is plotted in fig.13b. The AODs are seen to be higher than 0.01 on most of the occasions with frequent spikes reaching as high as 0.16. We considered different scenarios to explain such high AOD. These included, (i) volcanic perturbation to stratospheric AOD, and (ii) high altitude cirrus clouds at TTL region. We first compared these extinction coefficient and AOD values with the corresponding area-averaged values for the entire tropical belt (10^0S to 10^0N) (Kremser et al., 2016). The maximum value of stratospheric AOD averaged for the entire tropical belt (Kremser et al., 2016)
20 for the period 2000 to 2012 is marked with the dotted red-line in fig.13b. It can be seen that, the stratospheric AODs from our analysis over the 5 regional boxes are roughly 4-6 times higher than the background tropical stratospheric AOD (dotted red line, fig.13b), same is the case for aerosol extinction coefficient values as well (comparison not shown). This signifies the enhancement in the stratospheric aerosol burden over the regions under consideration, above the background stratospheric aerosol loading. One of the major controllers of stratospheric AOD is the in-flux of particulates namely sulphates, organics and
25 ash, and gases like SO$_2$ from volcanic eruptions into the stratosphere (Kremser et al., 2016). An examination of the occurrence of global volcanic eruptions from 2008 to 2012 (Kremser et al., 2016) suggests that, out of the 11 major volcanic eruptions that occurred during that period, 7 were centered away from the tropics. Also, the flux of SO$_2$ in the stratosphere from the most intense of the 11 events, was merely $(1/10)^{th}$ of that of the mount Pinatubo eruption (Kremser et al., 2016). Thus, this proposes that the enhancement in AOD and the extinction coefficient over the regions under consideration in this study may not
30 be linked to volcanic eruptions. The monsoon season (June to September) appears to be the favorite period for the lifted layers in the stratosphere (fig.13a). This looks to be linked to the vertical lifting associated with severe convection (as seen in our model simulations fig.11 and Mov.1 in supplementary material) and thin tropopause layer as explained earlier (Fu et al., 2006; Randel et al., 2010; Vernier et al., 2011; Thampi et al., 2012; Uma et al., 2012). Additionally, these layers seem to be present during the other seasons (pre-monsoon and winter) as well. The Indian region experiences a large scale ascending motion

above 10 km during winter months (Rao et al., 2008). Such an ascending motion can cause intrusion of tropospheric air (lying at 8-10 km) into the stratosphere (Rao et al., 2008). Thus, while the monsoonal convection and the related thermodynamics appears to be a cause for the summer time higher extinction coefficient values at stratospheric heights over the Indian region, the transport of tropospheric air mass into the stratosphere due to the large-scale ascent beyond 10 km looks to be responsible

5   for the winter time high values.

To throw light on the aerosol species responsible for such values of extinction coefficient, we examined the Particle Depolarization Ratios (at 550nm, henceforth PDR) at these altitudes (fig.13c). PDR is the ratio of attenuated backscatter coefficient in perpendicular direction to that in the parallel direction. We computed the PDR values from the corresponding backscatter coefficient values. The PDR values are seen to be higher than 0.3 on most of the occasions. This suggests the presence of

10   non-spherical aerosol species at those altitudes. One of the major non-spherical aerosol specie over this region is mineral dust. But dust is relatively too heavy and coarse to be lifted up to such altitudes. On the other hand, the maximum cloud top altitude occurring over the Indian region during the monsoon season is 20 km (Meenu et al., 2010). This suggests that, the non-spherical ice crystals emanating from the anvils of the convective towers over the Indian region could be found only around 20 km and not above 21-22 km. These together eliminate the possibility of presence of non-spherical mineral dust particles and ice crystals

15   at these heights. A few previous studies have noticed presence of BC chain agglomerates at the upper tropospheric and lower stratospheric heights (Blake and Kato, 1995; Bekki, 1997). Such a transport of BC to the stratospheric heights could be a result of convective-lifting (as seen in our model simulations fig.11 and Mov.1) and 'self-lifting' (de Laat et al., 2012) associated with them. Though pure and nascent BC has relatively lower value of PDR, the aged BC particles being porous (Chand et al., 2005; Dusek et al., 2005) and capable of forming long chain agglomerates are non-spherical and would depict higher values of

20   PDR. Such BC agglomerates even when mixed with stratospheric sulfate could still give rise to non-spherical shapes and thus higher values of PDR. This indicates the possible existence of BC at the stratospheric altitudes over the Indian region. Thus, the model simulated convective transport of high altitude aircraft emitted BC layers to UTLS region, favorable conditions for cross-tropopause transport of air-mass over Indian region during monsoonal months, large scale winter-time ascending motion above 10 km over Indian region and the presence of local BC emission sources (aircrafts) at high altitudes (~ 10km) throughout

25   the year together indicate the possibility of aircrafts emissions being primarily responsible for the possible presence of BC in stratosphere over the Indian region.

5   Possible implications of presence of BC at stratospheric heights

Our model simulations suggest that, aircrafts emissions are capable of producing the observed elevated aerosol layers in free troposphere (middle and upper) and the BC particles in these layers can intrude into the stratosphere, especially during periods

30   of thin TTL, aided by strong convective lofting (associated with summer monsoon) and self-lifting mechanisms. The average residence time of stratospheric aerosol is about 1 year (Snetsinger et al., 1987). BC aerosols, owing to their porosity and fractal shape (Blake and Kato, 1995; Bekki, 1997), can provide larger surface area to support heterogeneous chemical reactions in the upper troposphere and lower stratosphere. One of such reactions is the ozone decomposition on BC (Akhter et al., 1985;

Bekki, 1997; Schurath and Naumann, 1998; Disselkamp et al., 2000; Chughtai et al., 2003; Satheesh et al., 2013), which may result in depletion of stratospheric ozone. Besides, if BC is transported to the stratospheric heights, the high altitude cirrus clouds existing around the tropical tropopause layer, which reflect back most of the solar radiation incident on them, would consequently induce increased interaction between solar radiation and the lifted BC layer (Satheesh and Moorthy, 2005). This

5 would substantially enhance BC-induced warming of lower stratosphere. Since the atmosphere becomes increasingly thinner with altitude, for a given amount of absorbed energy, the warming would be higher at upper levels than that near the surface. Kamm et al. (1999), based on laboratory experiments, have reported that reaction rate of loss of ozone in presence of BC has positive temperature dependence. Thus, the aircraft emitted BC could possibly contribute to the depletion of the stratospheric ozone layer. The continued negative trend in stratospheric ozone over 40^0S-40^0N from 1984 to 2014 (Bourassa et al., 2014)

10 could possibly be related to the ever increasing aircraft traffic. The observed delays in recovery of stratospheric ozone hole (Kane, 2008, 2009), could also be influenced by such interactions of lifted BC with the stratospheric ozone.

6   Conclusions

The altitude distribution of BC in atmosphere plays a crucial role in deciding the BC-induced warming of the atmosphere. Such an atmospheric warming due to BC gets amplified when BC lies above strongly reflecting surface like clouds. The enhanced

15 warming of BC can give rise to local instability and subsequent vertical lifting. Such absorption-warming-convection cycle can transport BC to higher altitudes. On account of its absorbing nature, high altitude BC can burn-off cirrus clouds. Realizing the importance of the vertical profile of BC, Babu et al. (2011) measured vertical profile of BC over strongly convecting Indian region during pre-monsoon periods (March 2010) using high altitude zero pressure balloon. The authors reported 2 sharp and confined high altitude layers of BC at 4.5 km and 8.3 km. The existence of the high altitude BC layers was confirmed by

20 two subsequent balloon flights conducted during the subsequent winter and pre-monsoon seasons. While the high values of BC within 1st 3 km of atmosphere could be explained by boundary layer mixing, the higher BC values aloft appeared to be a mystery. The present study used the regional chemistry transport model - WRF-Chem, to understand the causes behind the observed high altitude sharp and confined BC layers. Firstly the simulations (incorporating surface BC emissions) of the meteorological parameters within the model were examined. Broad agreements of model simulated meteorological variables

25 with their corresponding observations from the balloon measurements were found. Then the model simulated vertical profile of BC were compared with the corresponding observed profile, but it was found that the model could not replicate the high altitude BC layers as seen in observations. Thus reasonable simulations of meteorology within the model could not give rise to the high altitude BC layers. Then the emission of BC from high altitude sources i.e. aircrafts were prescribed in our simulations. The aircraft BC emissions from MACCity inventory, interpolated to our model grids with necessary modifications were used for this

30 purpose. Upon the prescription of BC emissions from aircrafts, the model simulated vertical profile of BC started showing the mysterious high altitude BC peaks as seen in the observations. The sharp and confined nature of the simulated BC peaks showed large similarities with the observations, though their exact altitude and the magnitude differed vis-a-vis the observations. The fact that, aircraft emissions of BC being the primary cause behind the high altitude BC peaks, was re-confirmed when the

peaks remained undisturbed, even after shutting down the surface level emissions of BC. The corresponding atmospheric heating rates due to such observed and simulated profiles of BC were then computed. It was seen that such BC profiles could give rise to local instability and subsequent vertical mixing even at higher altitudes (∼10-11km). Such high altitude BC peaks would cause warming which could be amplified in the presence of highly reflecting clouds beneath them. This absorption-

5 warming-convection cycle could possibly lift BC to even higher altitudes. In addition to such a 'self-lifting', it was seen in a separate model simulation done for the monsoonal month of July that, such high altitude BC were transported vertically up by the underlying strong convection over the Indian region. The transport was seen to be as high as up to 17.6 km i.e. the UTLS region. Many previous studies have reported that the near-tropopause conditions over Indian region especially during monsoonal months are more favorable for the cross-tropopause transport of the tropospheric air-mass. Thus this could act as a

10 pathway for the lifted aircraft-emitted BC layers to reach the stratosphere. Many previous studies have also reported presence of BC in stratosphere. To understand this further, the vertical profiles of aerosol extinction coefficient from satellite measurements over the stratospheric heights across the Indian region were examined. The extinction coefficient values as high as $0.02 \, \text{km}^{-1}$, which were an order of magnitude greater than the average tropical stratospheric aerosol extinction coefficients were noticed. Though such layers were more visible during the monsoonal months, their presence during winters hinted at the possible co-

15 operation between self-lifting and large-scale ascent over Indian region, in bringing the layers in the UTLS region. On the further examination, it was found that the particle depolarization ratio corresponding to the high values extinction coefficient were higher than 0.3. Such high values of PDR signify non-spherical nature of the involved species. Eliminating the possibility of mineral dust particles and ice crystals being responsible for such high values of PDR and finding from previous studies about the presence of non-spherical BC chain agglomerates in the UTLS region, it was concluded that such BC structures would

20 possibly be responsible for the high values of PDR over the stratospheric altitudes. Once in stratosphere, BC can reside for a longer period of time due to the inherent stability of stratosphere and the absence of strong removal mechanisms. One of the possible implications of presence of BC in stratosphere is the reaction involving decomposition of ozone on BC, which would result in depletion of ozone. So potentially, the lifted upper tropospheric BC in stratosphere could harm the earth's protective blanket. Thus, while aircrafts look to be the cause for the sharp and confined high altitude layers of BC, such layers when lifted

25 to stratosphere (under favorable conditions), can potentially affect the ozone layer and can have significant implications for health of all living organisms. Realizing the potential of emissions from aircrafts, a recent article (Green-sky thinking , 2016) also advocates for regulations on aircraft emissions. More observational studies using satellite and stratospheric balloons, and modeling studies are required to address this important phenomena especially over regions of high aircraft activity.
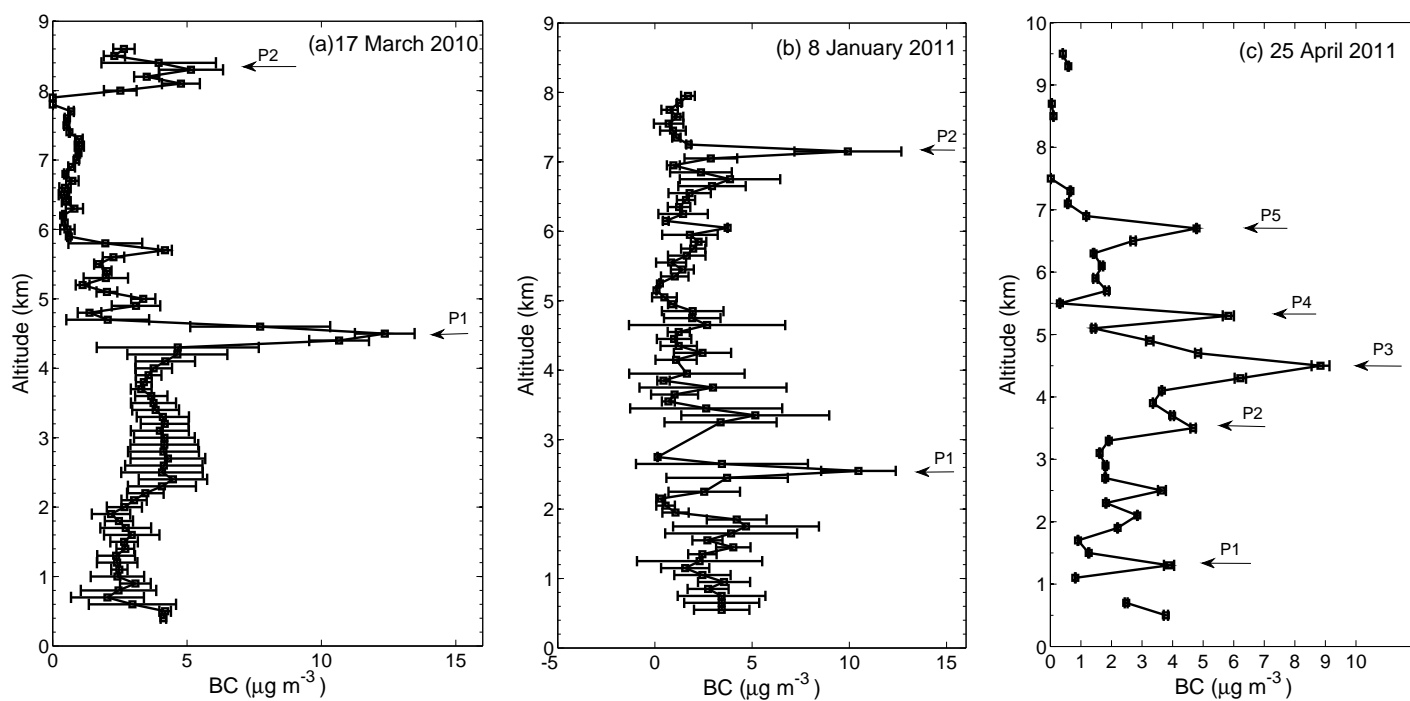
Figure 1. Observed vertical profile of BC over Hyderabad obtained from balloon measurements (a). during 17 March 2010 (b). during 8 January 2011 (c). during 25 April 2011. The high altitude BC peaks in each profile are identified by letters P1 to P5
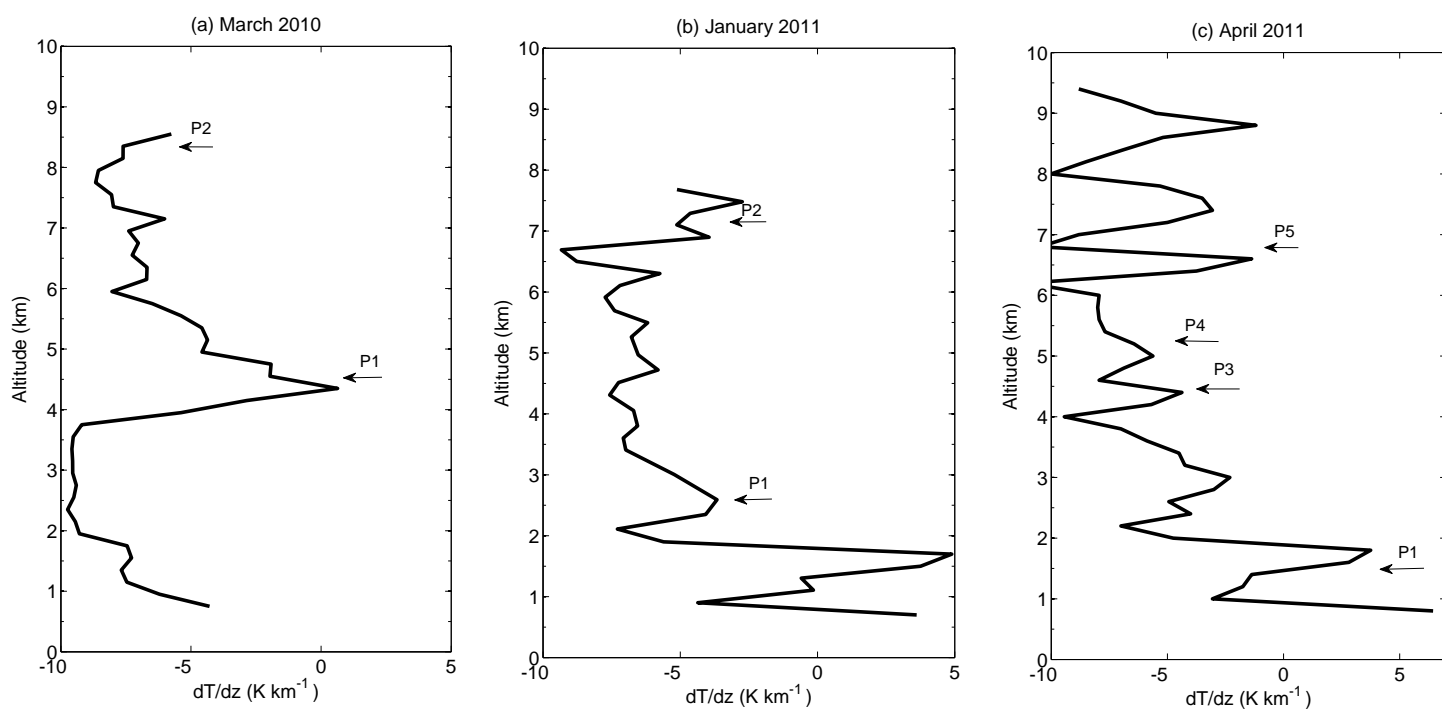
Figure 2. Observed vertical profile of dT/dz (K km^{-1}) over Hyderabad region obtained from balloon measurements (a). during 17 March 2010 (b). during 8 January 2011 (c). during 25 April 2011. The locations corresponding to high altitude BC peaks in fig.1 are identified in profile by letters P1 to P5.
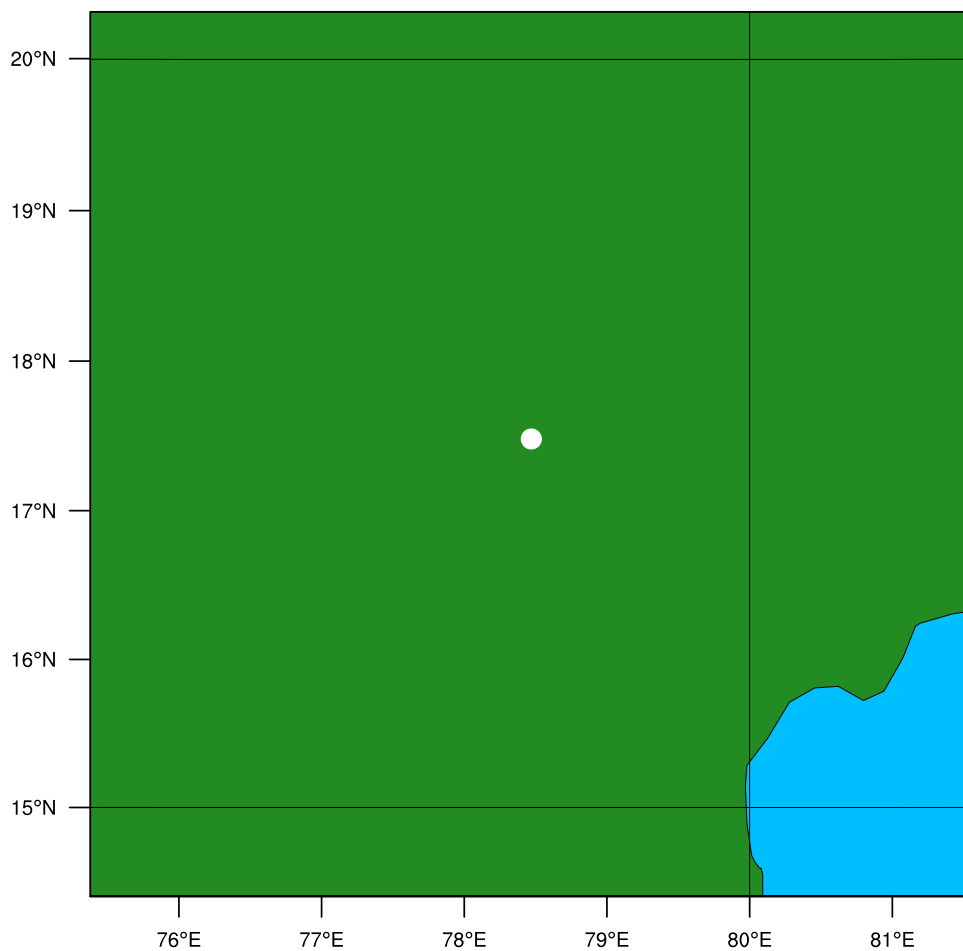
Figure 3. Model domain, Hyderabad is marked with a white dot. The blue area in the map indicates a part of Bay of Bengal.
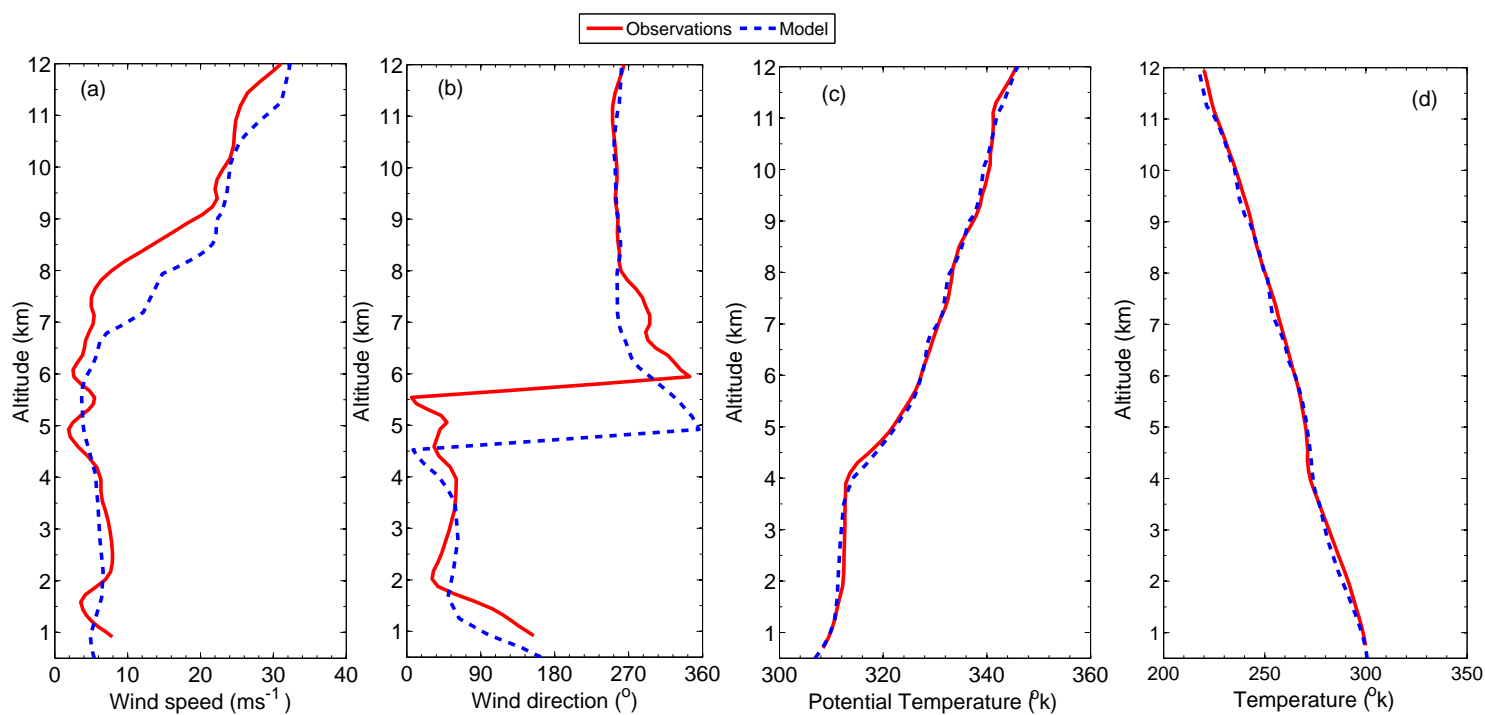
Figure 4. Comparison between the model simulated meteorological variables in NoACEM/Ctrl (control) run and the corresponding observations over the balloon flight region on 17, March 2010 for (a) wind speed (b) wind direction (c) Potential temperature (d) Temperature
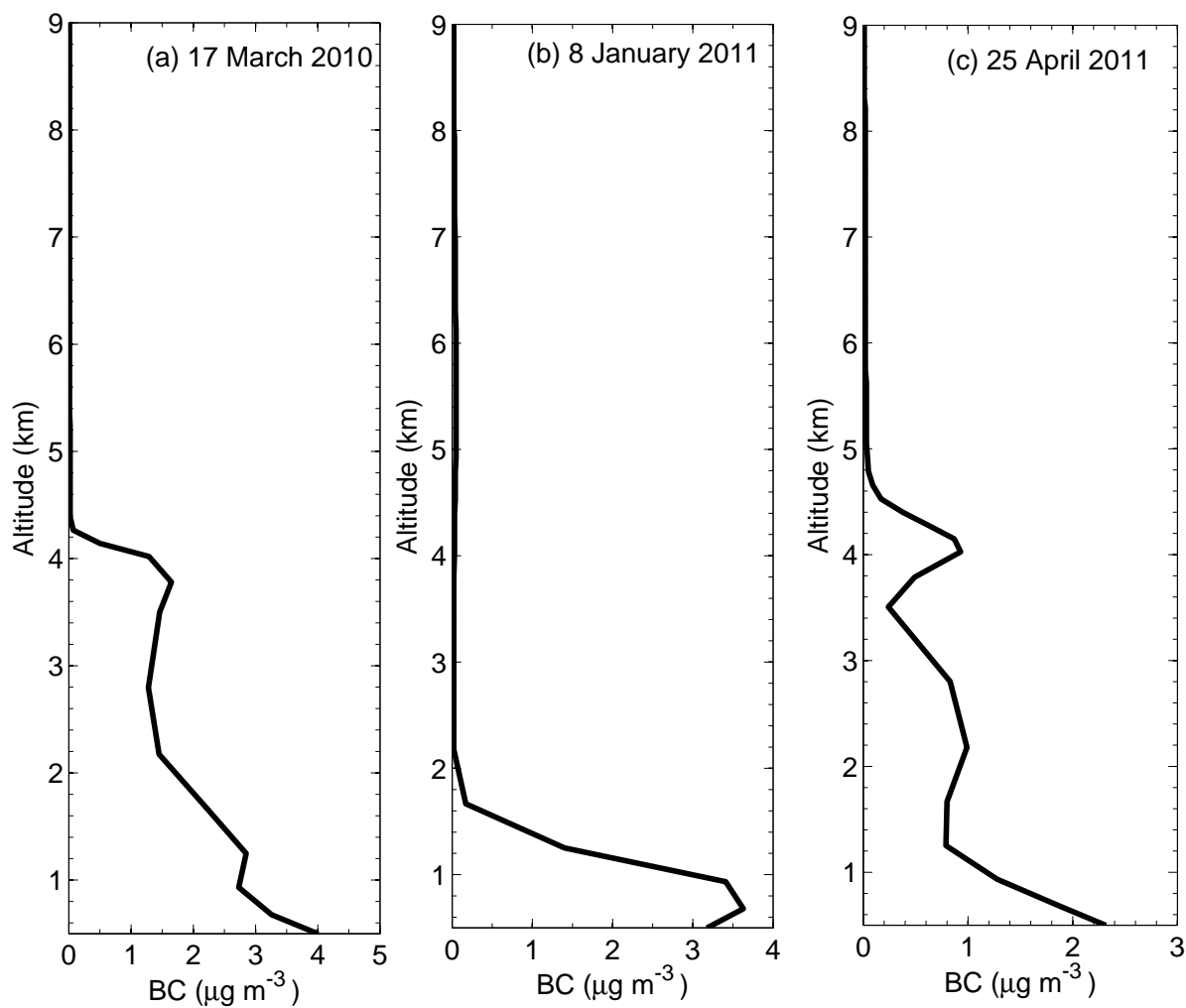
Figure 5. Model simulated vertical profile of BC over the balloon flight region in the NoACEM/Ctrl (control) run during (a). 17 March 2010, (b). 8 January 2011 and (c). 25 April 2011.
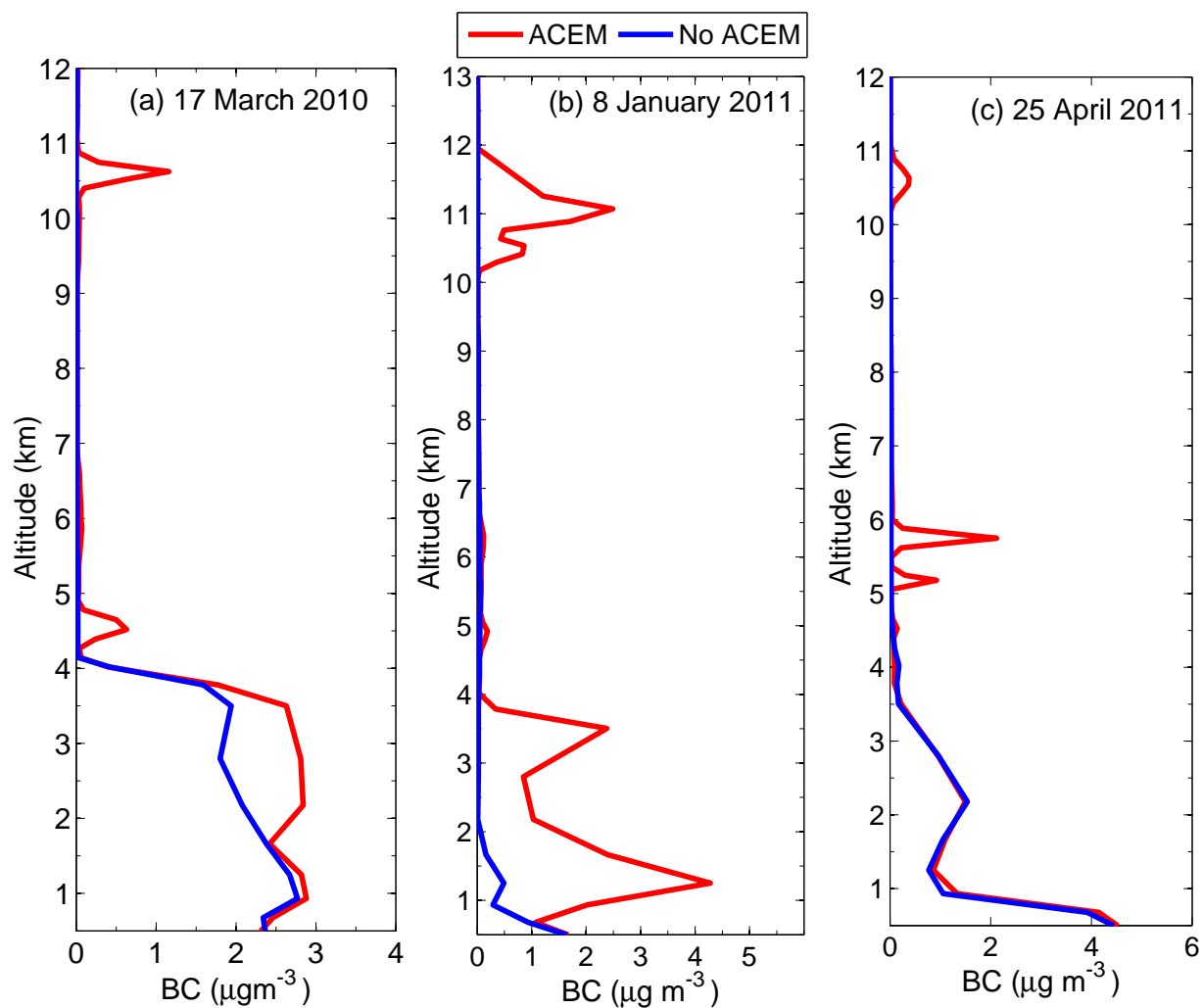
Figure 6. Model simulated vertical profile of BC over the area in the vicinity of the balloon flight region for (blue line) NoACEM/Ctrl (control run) and (red line) ACEM (runs with prescription of aircraft BC emssions) during (a). 17 March 2010, (b). 8 January 2011 and (c). 25 April 2011.
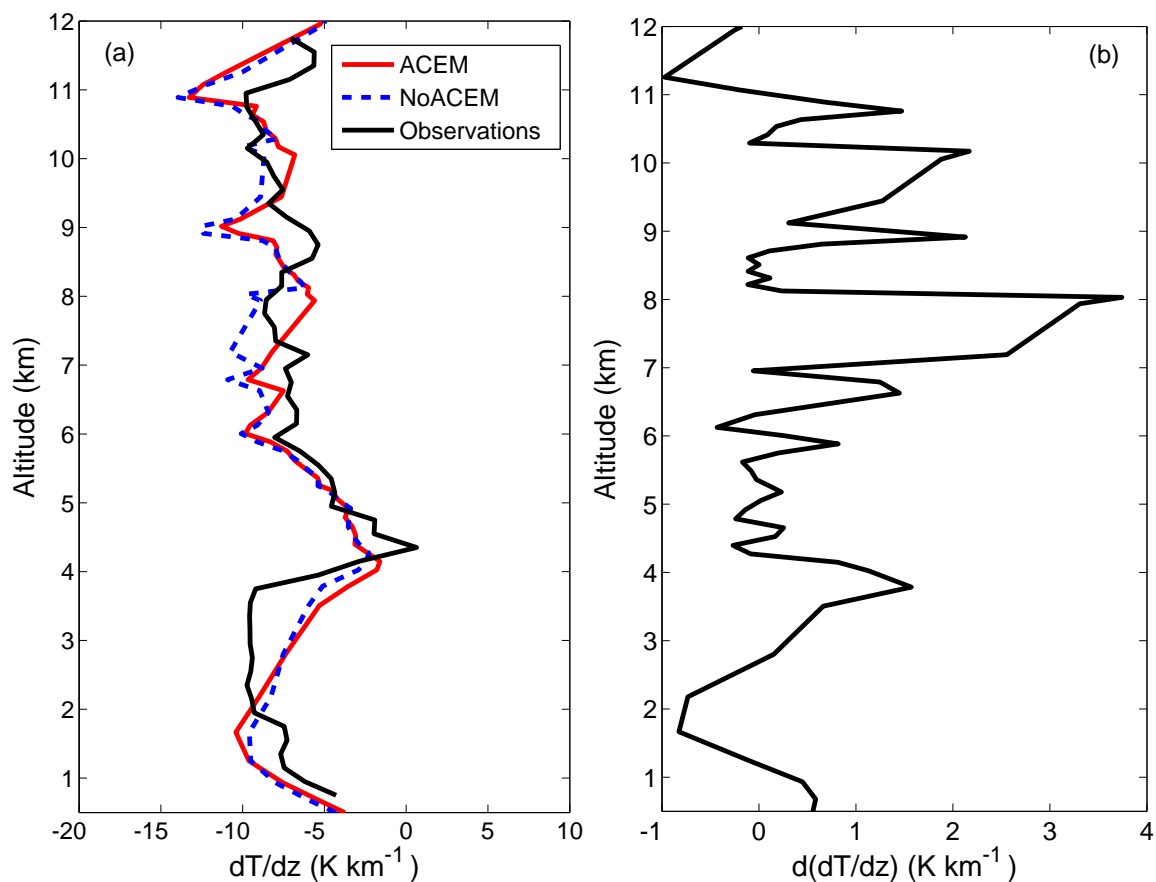
Figure 7. (a) Vertical profile of dT/dz (K km^{-1}) over the balloon flight region on 17, March 2010 from: (black-line)- Observations, (blue dashed line)- Simulations without BC emissions from aircrafts (NoACEM) and (red line)- Simulations with BC emissions from aircrafts (ACEM). (b) Vertical profile of difference in dT/dz values for 2 model simulations, d(dT/dz)= dT/dz$_{ACEM}$ - (dT/dz)$_{NoACEM}$
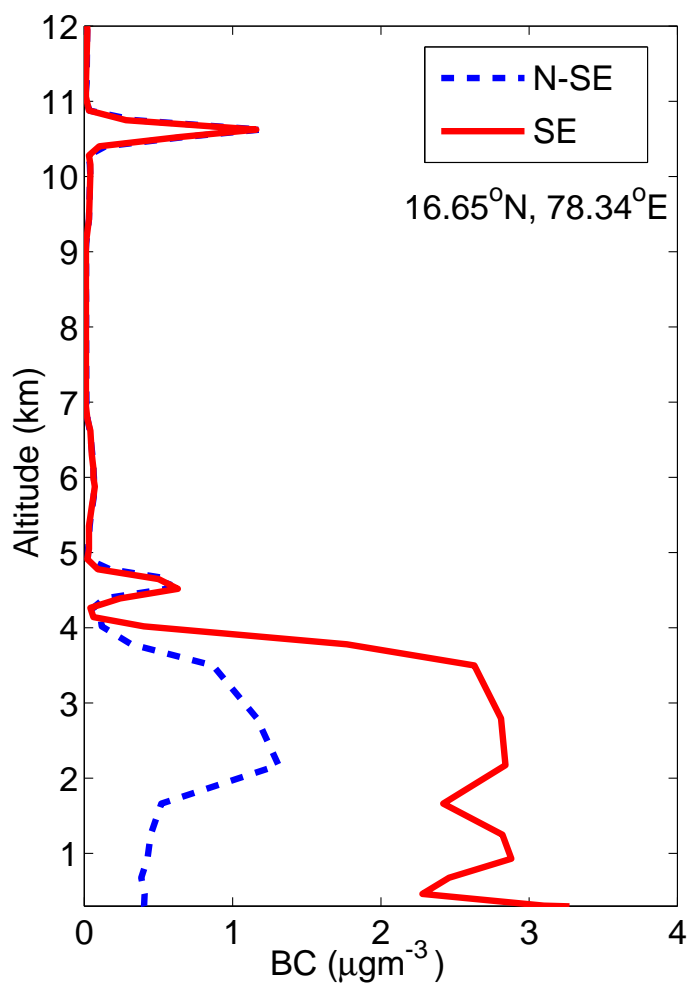
Figure 8. Model simulated vertical profile of BC during 17 March 2010 for (a). N-SE runs (model simulations without prescription of surface level anthropogenic BC emissions) (b). SE runs (model simulations with prescription of surface level anthropogenic BC emissions).
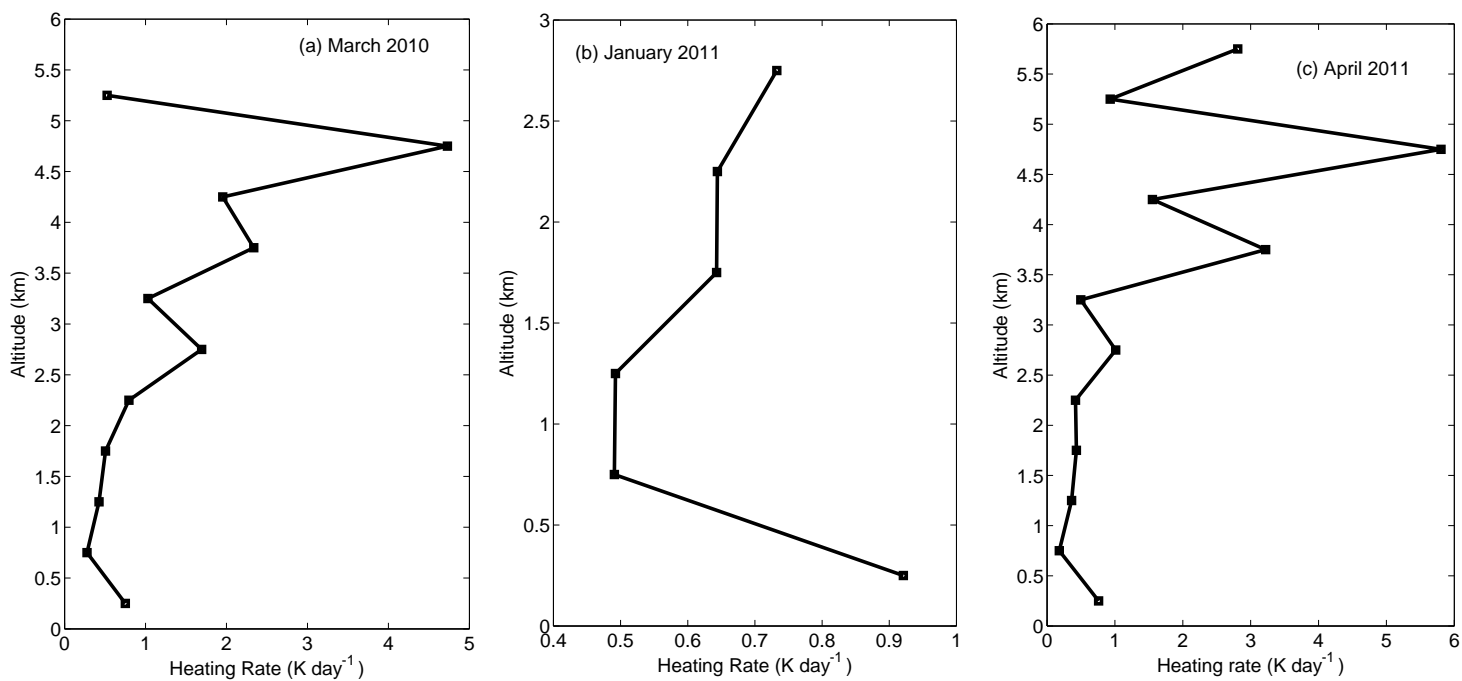
Figure 9. Vertical profiles of atmospheric heating rates for the observed BC profiles during (a).March 2010, (b). January 2011 and (c). April 2011.
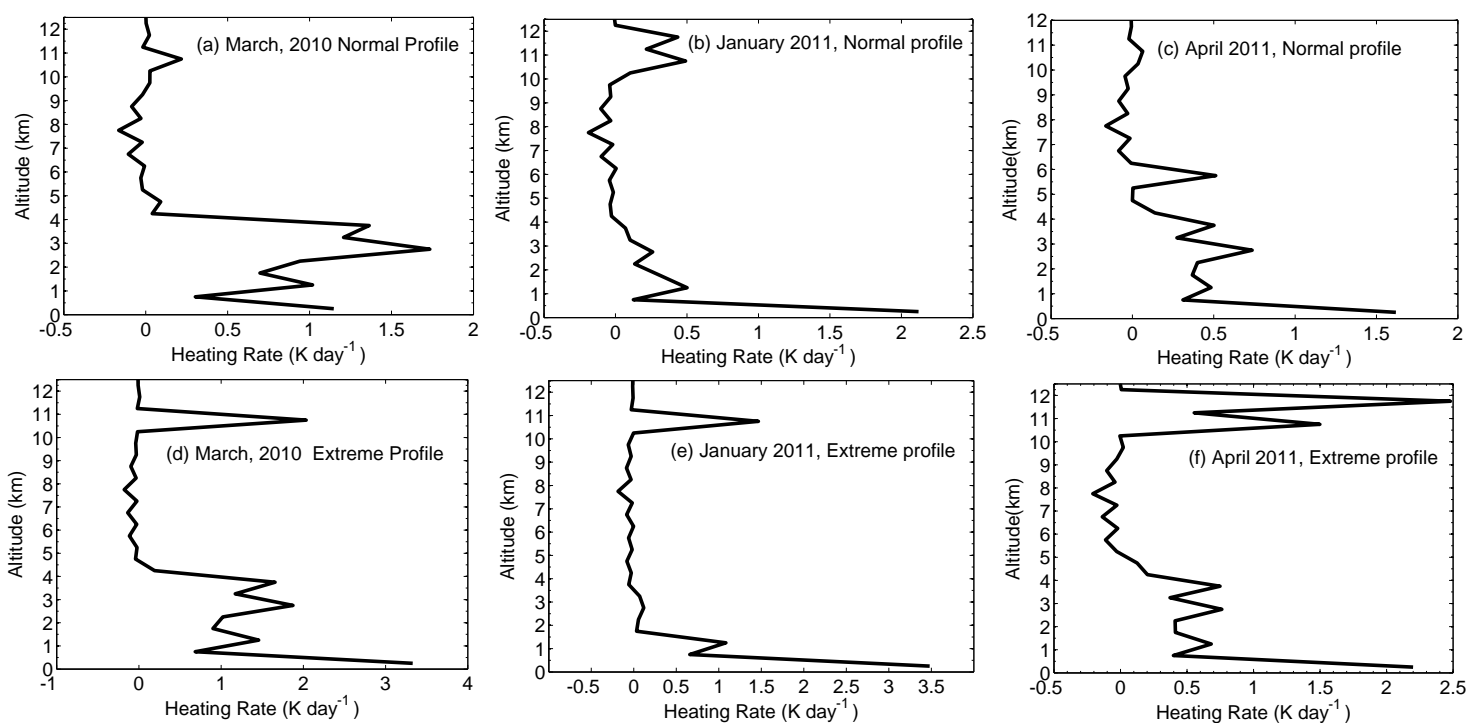
Figure 10. Vertical profiles of atmospheric heating rates for the model simulated BC profiles during (a and d). 17 March 2010 (b and e).8 January 2011 (c and f). 25 April 2011. Please refer section 4.6.2 for the meaning of the terms 'normal profile' and 'extreme profile'.
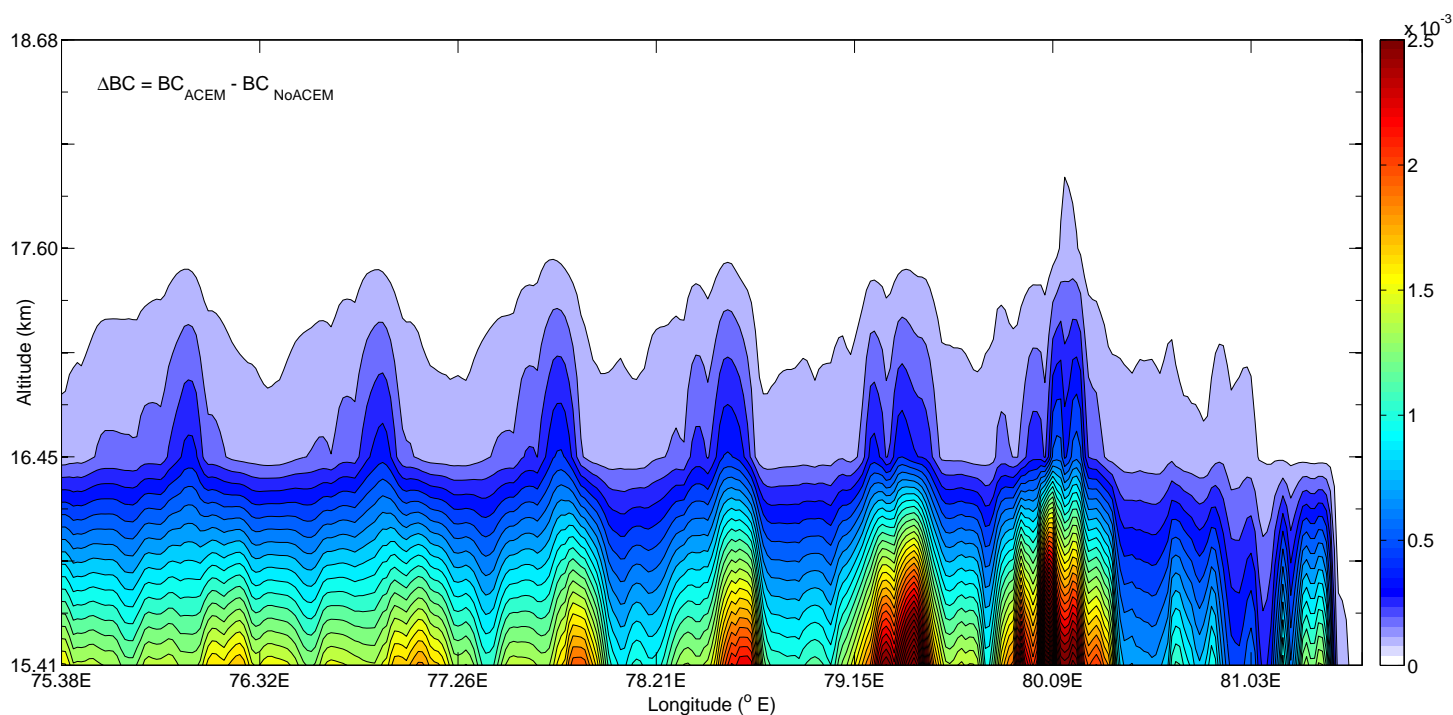
Figure 11. Vertical profile of the difference in BC mass concentration (μg m^{-3}) in ACEM runs vis-a-vis NoACEM run, averaged for the entire duration of the model simulation, carried out during July 2010. Here, ΔBC= BC$_{ACEM}$-BC$_{NoACEM}$.
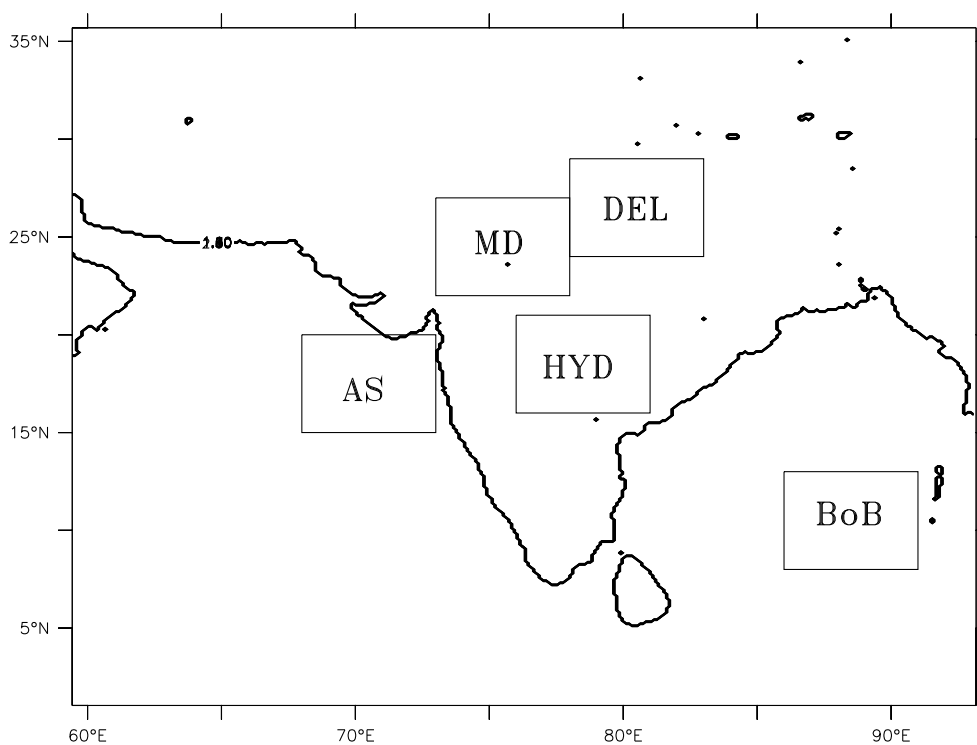
Figure 12. $5^0 \times 5^0$ regional boxes considered for the CALIPSO analysis (AS-Arabian sea, BoB-Bay of Bengal, HYD- Hyderabad, MD-Mumbai-Delhi and DEL-Delhi).
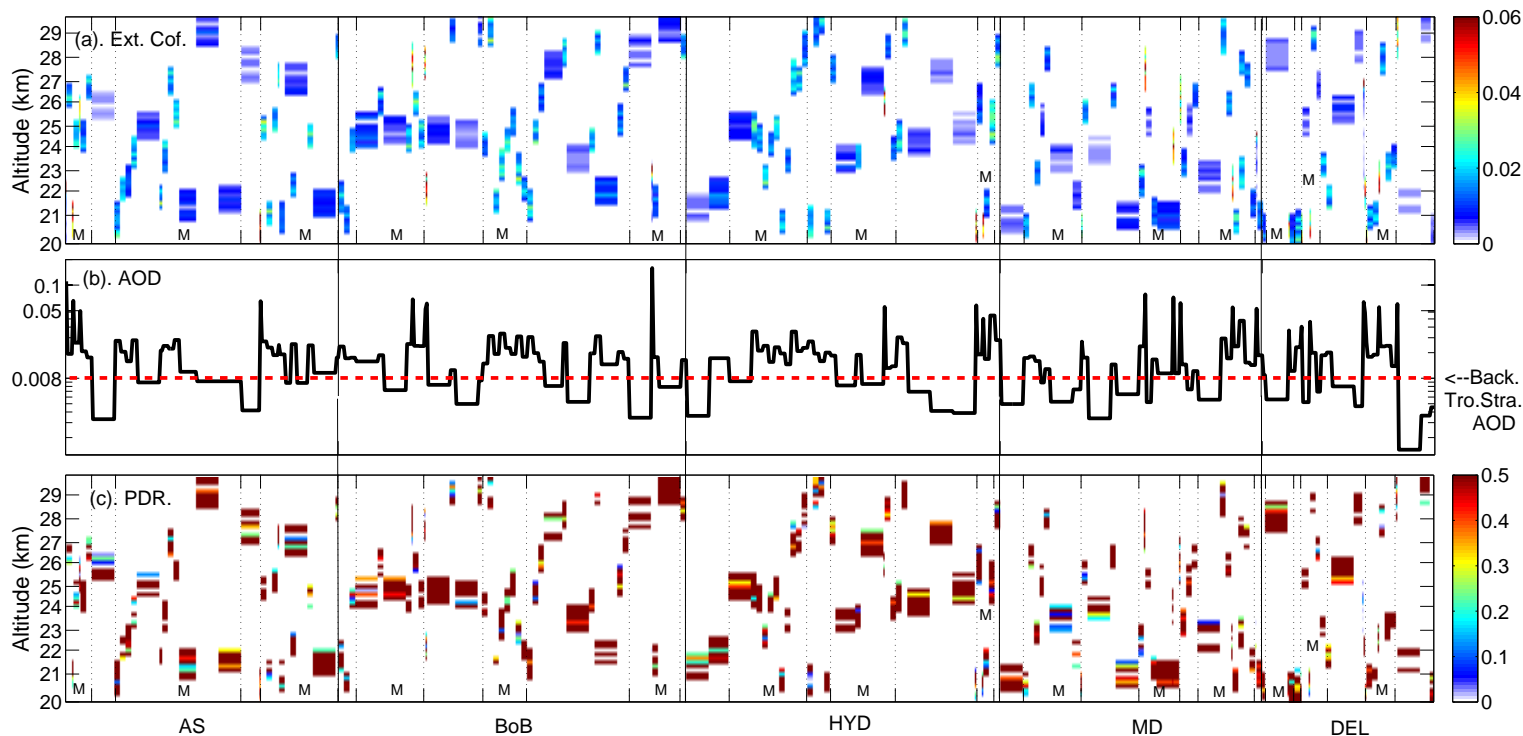
Figure 13. Time series of vertical profile of (a). Extinction coefficient over 5 regions (AS-Arabian sea, BoB- Bay of Bengal, HYD- Hyderabad, MD- Mumbai-Delhi and DEL-Delhi) over and around India (b). Corresponding stratospheric (from 20 km to ∼30 km) AOD, the background stratospheric AOD for the entire tropical belt (Kremser et al., 2016) is shown by the dotted red line (c). Particle Depolarization Ratio (PDR) over the same 5 regions from January 2010 to December 2012. The individual time series of Ext. Cof., AOD and PDR. of each region are appended together in the figure one after the other. The letter M signifies the Monsoon (JJAS) season during a year under consideration

7 Code availability

The simulations are done using an open source online regional chemistry transport model WRF-Chem, which is freely available at http://www2.mmm.ucar.edu/wrf/users/.

8 Data availability

5 The extinction coefficient level 2 data from CALIPSO is available freely on
https://eosweb.larc.nasa.gov/HBDOCS/langley_web_tool.html.

Competing interests. The authors declare that they have no conflict of interest

Acknowledgements. All the computations are conducted on the computational cluster funded jointly by Department of Science and Technologies FIST program (DST-FIST), Divecha Center for Climate Change and ARFI project of Indian Space Research Organisation (ISRO).
10 This work is partially supported by MoES (Grant No:MM/NERC-MoES-1/2014/002) under the South West Asian Aerosol Monsoon Interactions (SWAAMI) project. Authors would like to thank the Computational and Information Systems Laboratory (CISL-NCAR) for the Research Data Archive.

References

Ackerman, A. S., Toon, O. B., Stevens, D. E., Heymsfield, A. J., Ramanathan, V., and Welton, E. J.: Reduction of Tropical Cloudiness by Soot, Science, 288, 1042–1047, doi:10.1126/science.288.5468.1042, http://science.sciencemag.org/content/288/5468/1042, 2000.

Akhter, M. S., Chughtai, A. R., and Smith, D. M.: The Structure of Hexane Soot I: Spectroscopic Studies, Applied Spectroscopy, 39, 143–153, doi:10.1366/0003702854249114, http://asp.sagepub.com/content/39/1/143.abstract, 1985.

Andreae, M. O., Artaxo, P., Fischer, H., Freitas, S. R., Grégoire, J.-M., Hansel, A., Hoor, P., Kormann, R., Krejci, R., Lange, L., Lelieveld, J., Lindinger, W., Longo, K., Peters, W., de Reus, M., Scheeren, B., Silva Dias, M. A. F., Ström, J., van Velthoven, P. F. J., and Williams, J.: Transport of biomass burning smoke to the upper troposphere by deep convection in the equatorial region, Geophysical Research Letters, 28, 951–954, doi:10.1029/2000GL012391, http://dx.doi.org/10.1029/2000GL012391, 2001.

Babu, S. S., Satheesh, S. K., and Moorthy, K. K.: Aerosol radiative forcing due to enhanced black carbon at an urban site in India, Geophysical Research Letters, 29, 27–1–27–4, doi:10.1029/2002GL015826, http://dx.doi.org/10.1029/2002GL015826, 1880, 2002.

Babu, S. S., Satheesh, S. K., Moorthy, K. K., Dutt, C. B. S., Nair, V. S., Alappattu, D. P., and Kunhikrishnan, P. K.: Aircraft measurements of aerosol black carbon from a coastal location in the north-east part of peninsular India during ICARB, Journal of Earth System Science, 117, 263–271, doi:10.1007/s12040-008-0030-1, http://dx.doi.org/10.1007/s12040-008-0030-1, 2008.

Babu, S. S., Moorthy, K., and Satheesh, S.: Vertical and Horizontal Gradients in Aerosol Black Carbon and Its Mass Fraction to Composite Aerosols over the East Coast of Peninsular India from Aircraft Measurements, Advances in Meteorology, 2010, doi:10.1155/2010/812075, http://dx.doi.org/10.1155/2010/812075, 812075, 2010.

Babu, S. S., Moorthy, K. K., Manchanda, R. K., Sinha, P. R., Satheesh, S. K., Vajja, D. P., Srinivasan, S., and Kumar, V. H. A.: Free tropospheric black carbon aerosol measurements using high altitude balloon: Do BC layers build "their own homes" up in the atmosphere?, Geophysical Research Letters, 38, doi:10.1029/2011GL046654, http://dx.doi.org/10.1029/2011GL046654, l08803, 2011.

Baumgardner, D., Kok, G., and Raga, G.: Warming of the Arctic lower stratosphere by light absorbing particles, Geophysical Research Letters, 31, doi:10.1029/2003GL018883, http://dx.doi.org/10.1029/2003GL018883, l06117, 2004.

Bekki, S.: On the possible role of aircraft-generated soot in the middle latitude ozone depletion, Journal of Geophysical Research: Atmospheres, 102, 10 751–10 758, doi:10.1029/97JD00134, http://dx.doi.org/10.1029/97JD00134, 1997.

Blake, D. F. and Kato, K.: Latitudinal distribution of black carbon soot in the upper troposphere and lower stratosphere, Journal of Geophysical Research: Atmospheres, 100, 7195–7202, doi:10.1029/94JD03118, http://dx.doi.org/10.1029/94JD03118, 1995.

Bond, T. C., Doherty, S. J., Fahey, D. W., Forster, P. M., Berntsen, T., DeAngelo, B. J., Flanner, M. G., Ghan, S., Kärcher, B., Koch, D., Kinne, S., Kondo, Y., Quinn, P. K., Sarofim, M. C., Schultz, M. G., Schulz, M., Venkataraman, C., Zhang, H., Zhang, S., Bellouin, N., Guttikunda, S. K., Hopke, P. K., Jacobson, M. Z., Kaiser, J. W., Klimont, Z., Lohmann, U., Schwarz, J. P., Shindell, D., Storelvmo, T., Warren, S. G., and Zender, C. S.: Bounding the role of black carbon in the climate system: A scientific assessment, Journal of Geophysical Research: Atmospheres, 118, 5380–5552, doi:10.1002/jgrd.50171, http://dx.doi.org/10.1002/jgrd.50171, 2013.

Boucher, O., Randall, D., Artaxo, P., Bretherton, C., G., F., P., F., V.-M., K., Y., K., H., L., U., L., P., R., S.K., S., S., S., B., S., and X.Y., Z.: Clouds and Aerosols. In: Climate Change 2013: The Physical Science Basis. Contribution of Working Group I to the Fifth Assessment Report of the Intergovernmental Panel on Climate Change [Stocker, T.F., D. Qin, G.-K. Plattner, M. Tignor, S.K. Allen, J. Boschung, A. Nauels, Y. Xia, V. Bex and P.M. Midgley (eds.)], Cambridge University Press, Cambridge, United Kingdom and New York, NY, USA, pp. 571–658, doi:10.1017/CBO9781107415324.016, 2013.

Bourassa, A. E., Degenstein, D. A., Randel, W. J., Zawodny, J. M., Kyrölä, E., McLinden, C. A., Sioris, C. E., and Roth, C. Z.: Trends in stratospheric ozone derived from merged SAGE II and Odin-OSIRIS satellite observations, Atmospheric Chemistry and Physics, 14, 6983–6994, doi:10.5194/acp-14-6983-2014, http://www.atmos-chem-phys.net/14/6983/2014/, 2014.

Chakraborty, A., Satheesh, S. K., Nanjundiah, R. S., and Srinivasan, J.: Impact of absorbing aerosols on the simulation of climate over the Indian region in an atmospheric general circulation model, Annales Geophysicae, 22, 1421–1434, doi:10.5194/angeo-22-1421-2004, 2004.

Chand, D., Schmid, O., Gwaze, P., Parmar, R. S., Helas, G., Zeromskiene, K., Wiedensohler, A., Massling, A., and Andreae, M. O.: Laboratory measurements of smoke optical properties from the burning of Indonesian peat and other types of biomass, Geophysical Research Letters, 32, doi:10.1029/2005GL022678, http://dx.doi.org/10.1029/2005GL022678, l12819, 2005.

Chand, D., Wood, R., Anderson, T. L., Satheesh, S. K., and Charlson, R. J.: Satellite-derived direct radiative effect of aerosols dependent on cloud cover, Nature Geosci, 2, 181–184, doi:10.1038/ngeo437, http://www.nature.com/ngeo/journal/v2/n3/suppinfo/ngeo437_S1.html, 2009.

Chin, M., Ginoux, P., Kinne, S., Torres, O., Holben, B. N., Duncan, B. N., Martin, R. V., Logan, J. A., Higurashi, A., and Nakajima, T.: Tropospheric aerosol optical thickness from the GOCART model and comparisons with satellite and Sun photometer measurements, Journal of the Atmospheric Sciences, 59, 461–483, doi:10.1175/1520-0469(2002)059<0461:TAOTFT>2.0.CO;2, 2002.

Chuan, R. L. and Woods, D. C.: The appearance of carbon aerosol oarticles in the lower stratosphere, Geophysical Research Letters, 11, 553–556, doi:10.1029/GL011i005p00553, http://dx.doi.org/10.1029/GL011i005p00553, 1984.

Chughtai, A. R., Kim, J. M., and Smith, D. M.: The Effect of Temperature and Humidity on the Reaction of Ozone with Combustion Soot: Implications for Reactivity near the Tropopause, Journal of Atmospheric Chemistry, 45, 231–243, doi:10.1023/A:1024250505886, http://dx.doi.org/10.1023/A:1024250505886, 2003.

Das, S. S., Venkat Ratnam, M., Uma, K. N., Patra, A. K., Subrahmanyam, K. V., Girach, I. A., Suneeth, K. V., Kumar, K. K., and Ramkumar, G.: Stratospheric intrusion into the troposphere during the tropical cyclone Nilam (2012), Quarterly Journal of the Royal Meteorological Society, 142, 2168–2179, doi:10.1002/qj.2810, http://dx.doi.org/10.1002/qj.2810, 2016.

de Laat, A. T. J., Stein Zweers, D. C., Boers, R., and Tuinder, O. N. E.: A solar escalator: Observational evidence of the self-lifting of smoke and aerosols by absorption of solar radiation in the February 2009 Australian Black Saturday plume, Journal of Geophysical Research: Atmospheres, 117, doi:10.1029/2011JD017016, http://dx.doi.org/10.1029/2011JD017016, d04204, 2012.

Disselkamp, R. S., Carpenter, M. A., Cowin, J. P., Berkowitz, C. M., Chapman, E. G., Zaveri, R. A., and Laulainen, N. S.: Ozone loss in soot aerosols, Journal of Geophysical Research: Atmospheres, 105, 9767–9771, doi:10.1029/1999JD901189, http://dx.doi.org/10.1029/1999JD901189, 2000.

Dudhia, J.: Numerical Study of Convection Observed during the Winter Monsoon Experiment Using a Mesoscale Two-Dimensional Model, Journal of Atmospheric Science, 105, 3077–3107, 1989.

Dusek, U., Frank, G. P., Helas, G., Iinuma, Y., Zeromskiene, K., Gwaze, P., Hennig, T., Massling, A., Schmid, O., Herrmann, H., Wiedensohler, A., and Andreae, M. O.: "Missing" cloud condensation nuclei in peat smoke, Geophysical Research Letters, 32, doi:10.1029/2005GL022473, http://dx.doi.org/10.1029/2005GL022473, l11802, 2005.

Emmons, L. K., Walters, S., Hess, P. G., Lamarque, J.-F., Pfister, G. G., Fillmore, D., Granier, C., Guenther, A., Kinnison, D., Laepple, T., Orlando, J., Tie, X., Tyndall, G., Wiedinmyer, C., Baughcum, S. L., and Kloster, S.: Description and evaluation of the Model for Ozone and Related chemical Tracers, version 4 (MOZART-4), Geoscientific Model Development, 3, 43–67, doi:10.5194/gmd-3-43-2010, 2010.

Freitas, S.: Including the sub-grid scale plume rise of vegetation fires in low resolution atmospheric transport models, Atmospheric Chemistry Physics, 7, 3385–3398, 2007.

Freitas, S. R., Longo, K. M., Alonso, M. F., Pirre, M., Marecal, V., Grell, G., Stockler, R., Mello, R. F., and Sánchez Gácita, M.: PREP-CHEM-SRC – 1.0: a preprocessor of trace gas and aerosol emission fields for regional and global atmospheric chemistry models, Geoscientific Model Development, 4, 419–433, doi:10.5194/gmd-4-419-2011, http://www.geosci-model-dev.net/4/419/2011/, 2011.

Fromm, M., Bevilacqua, R., Servranckx, R., Rosen, J., Thayer, J. P., Herman, J., and Larko, D.: Pyro-cumulonimbus injection of smoke to the stratosphere: Observations and impact of a super blowup in northwestern Canada on 3–4 August 1998, Journal of Geophysical Research: Atmospheres, 110, doi:10.1029/2004JD005350, http://dx.doi.org/10.1029/2004JD005350, d08205, 2005.

Fu, R., Hu, Y., Wright, J. S., Jiang, J. H., Dickinson, R. E., Chen, M., Filipiak, M., Read, W. G., Waters, J. W., and Wu, D. L.: Short circuit of water vapor and polluted air to the global stratosphere by convective transport over the Tibetan Plateau, Proceedings of the National Academy of Sciences, 103, 5664–5669, doi:10.1073/pnas.0601584103, http://www.pnas.org/content/103/15/5664.abstract, 2006.

Fueglistaler, S., Dessler, A. E., Dunkerton, T. J., Folkins, I., Fu, Q., and Mote, P. W.: Tropical tropopause layer, Reviews of Geophysics, 47, doi:10.1029/2008RG000267, http://dx.doi.org/10.1029/2008RG000267, rG1004, 2009.

Gautam, R., Hsu, N. C., Lau, W. K.-M., and Yasunari, T. J.: Satellite observations of desert dust-induced Himalayan snow darkening, Geophysical Research Letters, 40, 988–993, doi:10.1002/grl.50226, http://dx.doi.org/10.1002/grl.50226, 2013.

Govardhan, G., Nanjundiah, R. S., Satheesh, S. K., Krishnamoorthy, K., and Kotamarthi, V. R.: Performance of WRF-Chem over Indian region: Comparison with measurements, Journal of Earth System Science, 124, 875–896, doi:10.1007/s12040-015-0576-7, http://dx.doi.org/10.1007/s12040-015-0576-7, 2015.

Govardhan, G. R., Nanjundiah, R. S., Satheesh, S., Moorthy, K. K., and Takemura, T.: Inter-comparison and performance evaluation of chemistry transport models over Indian region, Atmospheric Environment, 125, Part B, 486 – 504, doi:http://dx.doi.org/10.1016/j.atmosenv.2015.10.065, http://www.sciencedirect.com/science/article/pii/S1352231015304829, south Asian Aerosols And Anthropogenic Emissions: Regional And Global Climate Implications, 2016.

Green-sky thinking, Editorial, Nature, 530, 253–253, doi:10.1038/530253a, http://www.nature.com/news/green-sky-thinking-1.19376, 2016.

Haywood, J. M. and Shine, K. P.: The effect of anthropogenic sulfate and soot aerosol on the clear sky planetary radiation budget, Geophysical Research Letters, 22, 603–606, doi:10.1029/95GL00075, http://dx.doi.org/10.1029/95GL00075, 1995.

Herndon, S. C., Jayne, J. T., Lobo, P., Onasch, T. B., Fleming, G., Hagen, D. E., Whitefield, P. D., and Miake-Lye, R. C.: Commercial Aircraft Engine Emissions Characterization of in-Use Aircraft at Hartsfield-Jackson Atlanta International Airport, Environmental Science & Technology, 42, 1877–1883, doi:10.1021/es072029+, http://dx.doi.org/10.1021/es072029+, pMID: 18409607, 2008.

Hess, M., Koepke, P., and Schult, I.: Optical Properties of Aerosols and Clouds: The Software Package OPAC, Bulletin of the American Meteorological Society, 79, 831–844, doi:10.1175/1520-0477(1998)079<0831:OPOAAC>2.0.CO;2, http://dx.doi.org/10.1175/1520-0477(1998)079<0831:OPOAAC>2.0.CO;2, 1998.

Hong, S., Noh, Y., and Dudhia, J.: A New Vertical Diffusion Package with an Explicit Treatment of Entrainment Processes, Monthly Weather Review, 134, 2318–2341, doi:10.1175/1520-0493(2004)132<0519:EFOWPU>2.0.CO;2, 2006.

Hong, S.-Y.: A new stable boundary-layer mixing scheme and its impact on the simulated East Asian summer monsoon, Quarterly Journal of the Royal Meteorological Society, 136, 1481–1496, doi:10.1002/qj.665, http://dx.doi.org/10.1002/qj.665, 2010.

Kamm, S., Möhler, O., Naumann, K.-H., Saathoff, H., and Schurath, U.: The heterogeneous reaction of ozone with soot aerosol, Atmospheric Environment, 33, 4651 – 4661, doi:http://dx.doi.org/10.1016/S1352-2310(99)00235-6, http://www.sciencedirect.com/science/article/pii/S1352231099002356, 1999.

Kane, R.: Is ozone depletion really recovering?, Journal of Atmospheric and Solar-Terrestrial Physics, 70, 1455 – 1459, doi:http://dx.doi.org/10.1016/j.jastp.2008.04.012, http://www.sciencedirect.com/science/article/pii/S1364682608001107, 2008.

Kane, R.: Ozone depletion, worst not yet over, Indian J. Radio Space Phys., 38, 313–316, http://nopr.niscair.res.in/handle/123456789/6898, 2009.

Kompalli, S., Babu, S., N.B, B., and K.K., M.: Spring-time enhancement in aerosol burden over a high-altitude location in western trans-Himalaya: results from long-term observations, Curretn Science, 111, 117 – 131, doi:10.18520/cs/v111/i1/117-131, http://www.currentscience.ac.in/Volumes/111/01/0117.pdf, 2016.

Kremser, S., Thomason, L. W., von Hobe, M., Hermann, M., Deshler, T., Timmreck, C., Toohey, M., Stenke, A., Schwarz, J. P., Weigel, R., Fueglistaler, S., Prata, F. J., Vernier, J.-P., Schlager, H., Barnes, J. E., Antuña-Marrero, J.-C., Fairlie, D., Palm, M., Mahieu, E., Notholt, J., Rex, M., Bingen, C., Vanhellemont, F., Bourassa, A., Plane, J. M. C., Klocke, D., Carn, S. A., Clarisse, L., Trickl, T., Neely, R., James, A. D., Rieger, L., Wilson, J. C., and Meland, B.: Stratospheric aerosol—Observations, processes, and impact on climate, Reviews of Geophysics, 54, 278–335, doi:10.1002/2015RG000511, http://dx.doi.org/10.1002/2015RG000511, 2015RG000511, 2016.

Kuhlbusch, T. A. J., Andreae, M. O., Cachier, H., Goldammer, J. G., Lacaux, J.-P., Shea, R., and Crutzen, P. J.: Black carbon formation by savanna fires: Measurements and implications for the global carbon cycle, Journal of Geophysical Research: Atmospheres, 101, 23 651–23 665, doi:10.1029/95JD02199, http://dx.doi.org/10.1029/95JD02199, 1996.

Lamarque, J.-F., Bond, T. C., Eyring, V., Granier, C., Heil, A., Klimont, Z., Lee, D., Liousse, C., Mieville, A., Owen, B., Schultz, M. G., Shindell, D., Smith, S. J., Stehfest, E., Van Aardenne, J., Cooper, O. R., Kainuma, M., Mahowald, N., McConnell, J. R., Naik, V., Riahi, K., and van Vuuren, D. P.: Historical (1850–2000) gridded anthropogenic and biomass burning emissions of reactive gases and aerosols: methodology and application, Atmospheric Chemistry and Physics, 10, 7017–7039, doi:10.5194/acp-10-7017-2010, http://www.atmos-chem-phys.net/10/7017/2010/, 2010.

Lau, K., Kim, M., and Kim, K.: Asian summer monsoon anomalies induced by aerosol direct forcing: the role of the Tibetan Plateau, Climate Dynamics, 26, 855–864, doi:10.1007/s00382-006-0114-z, http://dx.doi.org/10.1007/s00382-006-0114-z, 2006.

Lau, W. K. M., Kim, M.-K., Kim, K.-M., and Lee, W.-S.: Enhanced surface warming and accelerated snow melt in the Himalayas and Tibetan Plateau induced by absorbing aerosols, Environmental Research Letters, 5, 025 204, http://stacks.iop.org/1748-9326/5/i=2/a=025204, 2010.

Liou, K.-N.: An introduction to atmospheric radiation, vol. 84, Academic press, 2002.

Meenu, S., Rajeev, K., Parameswaran, K., and Nair, A. K. M.: Regional distribution of deep clouds and cloud top altitudes over the Indian subcontinent and the surrounding oceans, Journal of Geophysical Research: Atmospheres, 115, doi:10.1029/2009JD011802, http://dx.doi.org/10.1029/2009JD011802, d05205, 2010.

Mlawer, E. J., Taubman, S. J., Brown, P. D., Iacono, M. J., and Clough, S. A.: Radiative transfer for inhomogeneous atmospheres: RRTM, a validated correlated-k model for the longwave, Journal of Geophysical Research: Atmospheres, 102, 16 663–16 682, doi:10.1029/97JD00237, 1997.

Moorthy, K. K., Babu, S. S., Sunilkumar, S. V., Gupta, P. K., and Gera, B. S.: Altitude profiles of aerosol BC, derived from aircraft measurements over an inland urban location in India, Geophysical Research Letters, 31, doi:10.1029/2004GL021336, http://dx.doi.org/10.1029/2004GL021336, l22103, 2004.

Nair, V., Babu, S. S., Moorthy, K. K., Sharma, A., Marinoni, A., and ., A.: Black carbon aerosols over the Himalayas: direct and surface albedo forcing, Tellus B, 65, doi:http://dx.doi.org/10.3402/tellusb.v65i0.19738, http://www.tellusb.net/index.php/tellusb/article/view/19738, 2013.

Nair, V. S., Babu, S. S., Gogoi, M. M., and Moorthy, K. K.: Large-scale enhancement in aerosol absorption in the lower free troposphere over continental India during spring, Geophysical Research Letters, 43, 11,453–11,461, doi:10.1002/2016GL070669, http://dx.doi.org/10.1002/2016GL070669, 2016GL070669, 2016.

Okada, K., Ikegami, M., Uchino, O., Nikaidou, Y., Zaizen, Y., Tsutsumi, Y., and Makino, Y.: Extremely high proportions of soot particles in the upper troposphere over Japan, Geophysical Research Letters, 19, 921–924, doi:10.1029/92GL00487, http://dx.doi.org/10.1029/92GL00487, 1992.

Olivier, J. G. J., Bouwman, A., Berdowski, J., Veldt, C., Bloos, J., Visschedijk, A., Zandveld, P., Haverlag, J., et al.: Description of EDGAR Version 2.0: A set of global emission inventories of greenhouse gases and ozone-depleting substances for all anthropogenic and most natural sources on a per country basis and on 1 degree x 1 degree grid, 1996.

Onasch, T. B., Jayne, J. T., Herndon, S., Worsnop, D. R., Miake-Lye, R. C., Mortimer, I. P., and Anderson, B. E.: Chemical Properties of Aircraft Engine Particulate Exhaust Emissions, Journal of Propulsion and Power, 25, 1121–1137, doi:10.2514/1.36371, http://dx.doi.org/10.2514/1.36371, 2009.

Petzold, A. and Schönlinner, M.: Multi-angle absorption photometry—a new method for the measurement of aerosol light absorption and atmospheric black carbon, Journal of Aerosol Science, 35, 421 – 441, doi:http://dx.doi.org/10.1016/j.jaerosci.2003.09.005, http://www.sciencedirect.com/science/article/pii/S0021850203004403, 2004.

Prijith, S., Babu, S. S., Lakshmi, N., Satheesh, S., and Moorthy, K. K.: Meridional gradients in aerosol vertical distribution over Indian Mainland: Observations and model simulations, Atmospheric Environment, 125, Part B, 337 – 345, doi:http://dx.doi.org/10.1016/j.atmosenv.2015.10.066, http://www.sciencedirect.com/science/article/pii/S1352231015304830, south Asian Aerosols And Anthropogenic Emissions: Regional And Global Climate Implications, 2016.

Pueschel, R. F., Boering, K. A., Verma, S., Howard, S. D., Ferry, G. V., Goodman, J., Allen, D. A., and Hamill, P.: Soot aerosol in the lower stratosphere: Pole-to-pole variability and contributions by aircraft, Journal of Geophysical Research: Atmospheres, 102, 13 113–13 118, doi:10.1029/96JD03061, http://dx.doi.org/10.1029/96JD03061, 1997.

Pusechel, R. F., Blake, D. F., Snetsinger, K. G., Hansen, A. D. A., Verma, S., and Kato, K.: Black carbon (soot) aerosol in the lower stratosphere and upper troposphere, Geophysical Research Letters, 19, 1659–1662, doi:10.1029/92GL01801, http://dx.doi.org/10.1029/92GL01801, 1992.

Qian, Y., Flanner, M. G., Leung, L. R., and Wang, W.: Sensitivity studies on the impacts of Tibetan Plateau snowpack pollution on the Asian hydrological cycle and monsoon climate, Atmospheric Chemistry and Physics, 11, 1929–1948, doi:10.5194/acp-11-1929-2011, http://www.atmos-chem-phys.net/11/1929/2011/, 2011.

Ramanathan, V. and Carmichael, G.: Global and regional climate changes due to black carbon, Nature Geosci, 1, 221–227, doi:10.1038/ngeo156, http://dx.doi.org/10.1038/ngeo156, 2008.

Ramanathan, V., Chung, C., Kim, D., Bettge, T., Buja, L., Kiehl, J., Washington, W., Fu, Q., Sikka, D., and Wild, M.: Atmospheric brown clouds: Impacts on South Asian climate and hydrological cycle, Proceedings of the National Academy of Sciences of the United States of America, 102, 5326–5333, doi:10.1073/pnas.0500656102, 2005.

Ramanathan, V., Ramana, M. V., Roberts, G., Kim, D., Corrigan, C., Chung, C., and Winker, D.: Warming trends in Asia amplified by brown cloud solar absorption, Nature, 448, 575–578, doi:10.1038/nature06019, http://www.nature.com/nature/journal/v448/n7153/suppinfo/nature06019_S1.html, 2007.

Randel, W. J., Park, M., Emmons, L., Kinnison, D., Bernath, P., Walker, K. A., Boone, C., and Pumphrey, H.: Asian Monsoon Transport of Pollution to the Stratosphere, Science, 328, 611–613, doi:10.1126/science.1182274, http://science.sciencemag.org/content/328/5978/611, 2010.

Rao, T., Uma, K. N., Narayana Rao, D., and Fukao, S.: Understanding the transportation process of tropospheric air entering the stratosphere from direct vertical air motion measurements over Gadanki and Kototabang, Geophysical Research Letters, 35, doi:10.1029/2008GL034220, http://dx.doi.org/10.1029/2008GL034220, l15805, 2008.

Ricchiazzi, P., Yang, S., Gautier, C., and Sowle, D.: SBDART: A Research and Teaching Software Tool for Plane-Parallel Radiative Transfer in the Earth's Atmosphere, Bulletin of the American Meteorological Society, 79, 2101–2114, doi:10.1175/1520-0477(1998)079<2101:SARATS>2.0.CO;2, http://dx.doi.org/10.1175/1520-04771998)079<2101:SARATS>2.0.CO;2, 1998.

Satheesh, S. and Moorthy, K. K.: Radiative effects of natural aerosols: A review, Atmospheric Environment, 39, 2089 – 2110, doi:http://dx.doi.org/10.1016/j.atmosenv.2004.12.029, http://www.sciencedirect.com/science/article/pii/S135223100500018X, 2005.

Satheesh, S. and Ramanathan, V.: Large differences in tropical aerosol forcing at the top of the atmosphere and Earth's surface, Nature, 405, 60–63, doi:10.1038/35011039, http://dx.doi.org/10.1038/35011039, 2000.

Satheesh, S., Moorthy, K. K., and Srinivasan, J.: New Directions: Elevated layers of anthropogenic aerosols aggravate stratospheric ozone loss?, Atmospheric Environment, 79, 879 – 882, doi:http://dx.doi.org/10.1016/j.atmosenv.2013.07.052, http://www.sciencedirect.com/science/article/pii/S1352231013005839, 2013.

Satheesh, S. K., Vinoj, V., and Moorthy, K. K.: Vertical distribution of aerosols over an urban continental site in India inferred using a micro pulse lidar, Geophysical Research Letters, 33, n/a–n/a, doi:10.1029/2006GL027729, http://dx.doi.org/10.1029/2006GL027729, l20816, 2006.

Satheesh, S. K., Moorthy, K. K., Babu, S. S., Vinoj, V., and Dutt, C. B. S.: Climate implications of large warming by elevated aerosol over India, Geophysical Research Letters, 35, n/a–n/a, doi:10.1029/2008GL034944, http://dx.doi.org/10.1029/2008GL034944, l19809, 2008.

Schultz, M., Backman, L., Balkanski, Y., Bjoerndalsaeter, S., Brand, R., Burrows, J., Dalsoeren, S., de Vasconcelos, M., Grodtmann, B., Hauglustaine, D., et al.: REanalysis of the TROpospheric chemical composition over the past 40 years (RETRO)–A long-term global modeling study of tropospheric chemistry, Final Report, Jülich/Hamburg, Germany, 2007.

Schurath, U. and Naumann, K.: Heterogeneous processes involving atmospheric particulate matter, Pure and Applied Chemistry, 70, 1353–1361, doi:https://doi.org/10.1351/pac199870071353, 1998.

Schwarz, J. P., Gao, R. S., Fahey, D. W., Thomson, D. S., Watts, L. A., Wilson, J. C., Reeves, J. M., Darbeheshti, M., Baumgardner, D. G., Kok, G. L., Chung, S. H., Schulz, M., Hendricks, J., Lauer, A., Kärcher, B., Slowik, J. G., Rosenlof, K. H., Thompson, T. L., Langford, A. O., Loewenstein, M., and Aikin, K. C.: Single-particle measurements of midlatitude black carbon and light-scattering aerosols from the boundary layer to the lower stratosphere, Journal of Geophysical Research: Atmospheres, 111, doi:10.1029/2006JD007076, http://dx.doi.org/10.1029/2006JD007076, d16207, 2006.

Sheridan, P. J., Brock, C. A., and Wilson, J. C.: Aerosol particles in the upper troposphere and lower stratosphere: Elemental composition and morphology of individual particles in northern midlatitudes, Geophysical Research Letters, 21, 2587–2590, doi:10.1029/94GL01387, http://dx.doi.org/10.1029/94GL01387, 1994.

Smirnova, T. G., Brown, J., and M.Benjamin, S. G.: Performance of Different Soil Model Configurations in Simulating Ground Surface Temperature and Surface Fluxes, Monthly Weather Review, 125, 1870–1884, doi:10.1175/1520-0493(1997)125<1870:PODSMC>2.0.CO;2, 1997.

Smirnova, T. G., Brown, J. M., Benjamin, S. G., and Kim, D.: Parameterization of cold-season processes in the MAPS land-surface scheme, Journal of Geophysical Research: Atmospheres, 105, 4077–4086, doi:10.1029/1999JD901047, 2000.

Snetsinger, K. G., Ferry, G. V., Russell, P. B., Pueschel, R. F., Oberbeck, V. R., Hayes, D. M., and Fong, W.: Effects of El Chichón on stratospheric aerosols late 1982 to early 1984, Journal of Geophysical Research: Atmospheres, 92, 14 761–14 771, doi:10.1029/JD092iD12p14761, http://dx.doi.org/10.1029/JD092iD12p14761, 1987.

Stettler, M., Eastham, S., and Barrett, S.: Air quality and public health impacts of {UK} airports. Part I: Emissions, Atmospheric Environment, 45, 5415 – 5424, doi:http://dx.doi.org/10.1016/j.atmosenv.2011.07.012, http://www.sciencedirect.com/science/article/pii/S135223101100728X, 2011.

Stettler, M. E. J., Boies, A. M., Petzold, A., and Barrett, S. R. H.: Global Civil Aviation Black Carbon Emissions, Environmental Science & Technology, 47, 10 397–10 404, doi:10.1021/es401356v, http://dx.doi.org/10.1021/es401356v, pMID: 23844612, 2013.

Strawa, A. W., Drdla, K., Ferry, G. V., Verma, S., Pueschel, R. F., Yasuda, M., Salawitch, R. J., Gao, R. S., Howard, S. D., Bui, P. T., Loewenstein, M., Elkins, J. W., Perkins, K. K., and Cohen, R.: Carbonaceous aerosol (soot) measured in the lower stratosphere during POLARIS and its role in stratospheric photochemistry, Journal of Geophysical Research: Atmospheres, 104, 26 753–26 766, doi:10.1029/1999JD900453, http://dx.doi.org/10.1029/1999JD900453, 1999.

Sunilkumar, S. V., Babu, A., and Parameswaran, K.: Mean structure of the tropical tropopause and its variability over the Indian longitude sector, Climate Dynamics, 40, 1125–1140, doi:10.1007/s00382-012-1496-8, http://dx.doi.org/10.1007/s00382-012-1496-8, 2013.

Thampi, B. V., Parameswaran, K., and Sunilkumar, S.: Semitransparent cirrus clouds in the upper troposphere and their contribution to the particulate scattering in the tropical {UTLS} region, Journal of Atmospheric and Solar-Terrestrial Physics, 74, 1 – 10, doi:http://dx.doi.org/10.1016/j.jastp.2011.09.005, http://www.sciencedirect.com/science/article/pii/S1364682611002598, 2012.

Thompson, G., Rasmussen, R. M., and Manning, K.: Explicit forecasts of winter precipitation using an improved bulk microphysics scheme. Part I: Description and sensitivity analysis, Monthly Weather Review, 132, 519–542, doi:10.1175/1520-0493(2004)132<0519:EFOWPU>2.0.CO;2, 2004.

Timko, M. T., Onasch, T. B., Northway, M. J., Jayne, J. T., Canagaratna, M. R., Herndon, S. C., Wood, E. C., Miake-Lye, R. C., and Knighton, W. B.: Gas Turbine Engine Emissions—Part II: Chemical Properties of Particulate Matter, Journal of Engineering for Gas Turbines and Power, 132, 061 505–061 505–15, doi:10.1115/1.4000132, http://dx.doi.org/10.1115/1.4000132, 2010.

Uma, K. N., Kumar, K. K., Shankar Das, S., Rao, T. N., and Satyanarayana, T. M.: On the Vertical Distribution of Mean Vertical Velocities in the Convective Regions during the Wet and Dry Spells of the Monsoon over Gadanki, Monthly Weather Review, 140, 398–410, doi:10.1175/MWR-D-11-00044.1, http://dx.doi.org/10.1175/MWR-D-11-00044.1, 2012.

Vernier, J.-P., Thomason, L. W., and Kar, J.: CALIPSO detection of an Asian tropopause aerosol layer, Geophysical Research Letters, 38, doi:10.1029/2010GL046614, http://dx.doi.org/10.1029/2010GL046614, l07804, 2011.

Wiedinmyer, C., Akagi, S. K., Yokelson, R. J., Emmons, L. K., Al-Saadi, J. A., Orlando, J. J., and Soja, A. J.: The Fire INventory from NCAR (FINN): a high resolution global model to estimate the emissions from open burning, Geoscientific Model Development, 4, 625–641, doi:10.5194/gmd-4-625-2011, http://www.geosci-model-dev.net/4/625/2011/, 2011.

Wild, O., Zhu, X., and Prather, M.: Fast-J: Accurate Simulation of In- and Below-Cloud Photolysis in Tropospheric Chemical Models, Journal of Atmospheric Chemistry, 37, 245–282, doi:10.1023/A:1006415919030, 2000.

Yasunari, T. J., Bonasoni, P., Laj, P., Fujita, K., Vuillermoz, E., Marinoni, A., Cristofanelli, P., Duchi, R., Tartari, G., and Lau, K.-M.: Estimated impact of black carbon deposition during pre-monsoon season from Nepal Climate Observatory – Pyramid data and

snow albedo changes over Himalayan glaciers, Atmospheric Chemistry and Physics, 10, 6603–6615, doi:10.5194/acp-10-6603-2010, http://www.atmos-chem-phys.net/10/6603/2010/, 2010.